The Response of the Atlantic Meridional Overturning Circulation to heat flux forcing in the Kiel Climate Model

by

Annika Reintges

(Matriculation number 883340)

presented to the faculty of
Mathematics and Natural Science of the
Christian-Albrechts-Universität zu Kiel
for the degree
Master of Science in
Climate Physics

First supervisor: Prof. Dr. Mojib Latif
Second supervisor: Dr. Thomas Martin

Kiel, January 2014

CONTENTS

ABSTRACT / ZUSAMMENFASSUNG 5

ABSTRACT 5

ZUSAMMENFASSUNG 7

I) INTRODUCTION 9

II) DATA & METHODS 14

DATA 14

METHODS 16

III) RESULTS 19

DYNAMICAL MECHANISMS 19

DOMINANT MODES 27

CONTROL EXPERIMENT 36

IV) SUMMARY & DISCUSSION 44

V) APPENDIX 50

VI) REFERENCES 63

VII) STATEMENT OF ORIGINALITY 68

ABSTRACT

The response of the Atlantic Meridional Overturning Circulation (AMOC) to heat flux forcing of the North Atlantic Oscillation (NAO) is analyzed. This is done with the Kiel Climate Model (KCM), a coupled ocean-atmosphere-sea ice model. The dynamical links of the atmosphere-ocean interaction in this experiment agree with other studies and theoretical considerations: In a positive (negative) NAO phase the enhanced (reduced) heat loss from the subpolar North Atlantic to the atmosphere leads to a deepening (shallowing) of the mixed layer, especially over the center of the subpolar gyre. This causes increased (decreased) convection and after 3 to 14 years a stronger (weaker) AMOC at 30°N.

The NAO forcing has a slightly red spectrum. The AMOC, however, responds with lower frequencies. For the AMOC index at 30°N two modes of variability can be identified through Singular Spectrum Analysis (SSA): one with a period of 93 years and one with a period of 36 years. However, general differences of these two modes in the spatial structure of the overturning streamfunction cannot be identified. Though, the longer mode might be related to anomalies in the mixed layer depth and the strength of the subpolar gyre, which exhibit variability on similar time scales.

To compare the conditions of an unforced simulation, a control experiment is also investigated. Here, the relation between the NAO and the AMOC is not as clear. The largest correlation is found when the AMOC 30°N index leads the NAO index by 1 year. Additionally, the temporal variability of the AMOC modes differs in this experiment. A low-frequency but unstable variability mode of about 120 years period is detected mainly for the first half of the simulation period. All other modes of the control experiment were interannual to decadal. This disagrees with a different control experiment version of the KCM, where a multi-centennial, a quasi-centennial, and a multi-decadal mode were dominant.

Furthermore, one must bear in mind that the KCM sea surface temperatures of the North Atlantic are biased. Too low temperatures, the resulting coverage of the Labrador Sea with sea ice, but also further differences of the model compared to observations might cause the missing convection in the Labrador Sea. This region, however, is often highlighted to play a crucial role for deep water formation and therefore for the strength of the AMOC. A reduction of these errors might lead to a better understanding of the AMOC and its variability modes. This finally helps to evaluate which modes could be excited or damped under future climate conditions.

ZUSAMMENFASSUNG

In dieser Arbeit wird die Reaktion der atlantischen meridionalen Umwälzzirkulation (engl. Atlantic Meridional Overturning Circulation - Abkz. AMOC) auf den Wärmefluss der Nord Atlantischen Oszillation (NAO) untersucht. Hierfür werden Daten des Kiel Climate Model (KCM) genutzt, welches ein gekoppeltes Modell ist und aus den Komponenten Ozean, Atmosphäre, und Meereis besteht.

Die dynamischen Zusammenhänge der Ozean-Atmosphären Wechselwirkung in diesem Experiment stimmen mit anderen Studien und theoretischen Überlegungen überein: In einer positiven (negativen) Phase der NAO führt der erhöhte (reduzierte) Wärmeverlust des subpolaren Nordatlantiks an die Atmosphäre zu einer tieferen (flacheren) ozeanischen Deckschicht, was sich besonders im Zentrum des Subpolarwirbels zeigt. Dies verursacht höhere (niedrigere) Konvektionsraten und nach 3 bis 14 Jahren schließlich eine stärkere (schwächere) AMOC bei 30°N.

Das Spektrum des NAO Antriebs ist leicht „rot“. Die Variabilität der AMOC allerdings reagiert mit tieferen Frequenzen. Durch Sigular Spectrum Analysis (SSA) können für den AMOC Index bei 30°N zwei dominante Variabilitätsmoden identifiziert werden: eine mit einer Periode von 93 Jahren und eine mit einer Periode von 36 Jahren. Generelle Unterschiede zwischen diesen beiden Moden können in der räumlichen Struktur der Umwälzzirkulation allerdings nicht festgestellt werden. Jedoch könnte die längere Mode mit Schwankungen der ozeanischen Deckschicht und der Stärke des Subpolarwirbels verbunden sein, die ähnlich lange Perioden aufweisen.

Um diese Bedingungen auch in einer Simulation ohne externen Antrieb zu testen, wird auch ein Kontroll-Experiment untersucht. In diesem ist die Verbindung zwischen NAO und AMOC nicht so deutlich. Bedeutende Korrelationen erhält man, wenn der AMOC Index den NAO Index mit einem Abstand von einem Jahr führt. Auch die Moden der AMOC Variabilität unterscheiden sich. Eine langwellige aber instabile Mode mit einer Periode von etwa 120 Jahren ist vor allem in der ersten Hälfte der Integration präsent. Alle anderen Moden des Kontroll-Experiments sind interannual bis dekadisch. Dieses Ergebnis unterscheidet sich von dem einer anderen Kontroll-Experiment Version des KCM, bei dem drei dominante Moden mit Perioden von mehreren Jahrhunderten, von etwa einem Jahrhundert, und mehreren Jahrzehnten identifiziert wurden.

Außerdem sollte man beachten, dass im KCM die Nordatlantischen Oberflächentemperaturen systematische Abweichungen aufweisen. Die zu niedrigen Temperaturen, die dadurch entstehende Bedeckung der Labrador See mit Meereis und weitere Unterschiede zu den Beobachtungen könnten die Ursache für die fehlende Konvektion in der Labrador See sein. Gerade diese Region aber wird oft als bedeutend hervorgehoben, wenn es um die Entstehung von Tiefenwasser und um die Stärke der AMOC geht. Eine Reduzierung dieser Fehler könnte zu einem besseren Verständnis der AMOC und ihrer Variabilitätsmoden führen. Dadurch könnte es schließlich ermöglicht werden einzuschätzen, welche dieser Model im zukünftigen Klima angeregt oder gedämpft werden.

I) INTRODUCTION

The North Atlantic Ocean is subject to external and internal variability. External variability is caused by changes in external conditions as, for example, greenhouse gas related heating. In contrast, internal variability is created within the climate system itself without any changes in boundary conditions. The non-linearity of the dynamical system and the heat exchange between the atmosphere and the ocean lead to variability that is caused internally. These fluctuations can be of stochastic nature without any persistence in time or space but they can also be part of climate modes associated with certain patterns or periods of variability.

In the atmosphere one of these dominant modes over the northern hemisphere is the North Atlantic Oscillation (NAO). Its phase depends on the difference between the low pressure center located over Iceland and the high pressure center located over the Azores. A positive phase is defined by an anomalously large pressure difference. This leads to increased westerlies and a northward shift of the storm tracks over the North Atlantic. Finally, it influences the temperature and precipitation conditions (e.g., Walker, 1924). A positive NAO phase, for example, causes mild and wet winters over northern Europe but lower precipitation in the Mediterranean region.

Ocean and atmosphere are coupled by surface heat flux, freshwater flux, and momentum flux. Thus, anomalies in the surface fluxes caused by the NAO are transferred into the ocean (e.g., Bjerknes, 1964). The anomalies in the surface heat flux pattern, for example, influence the sea surface temperature (SST) but also upper-ocean heat content, the mixed layer depth, and the subpolar gyre strength. The mixed layer depth is the depth up to which the potential density of the surface is sustained. It can become very deep in winter when a large heat release to the atmosphere causes cool and dense surface waters, which leads to instability and subsequent mixing. The North Atlantic subpolar gyre is a horizontally closed circulation with a low pressure center. It is set up by the large scale wind pattern but its strength can also be affected by anomalies in temperature. Cooling of the gyre during a positive NAO phase, for example, leads to an even lower pressure in the center and following geostrophic balance the speed of the gyre must increase.

The main influences of momentum flux anomalies are changes in the Ekman and sea ice transport. These and further effects of the NAO on the ocean are summarized in Visbeck et al. (2003). Also the mechanisms affecting the deeper ocean circulation are described by them:

Buoyancy flux is controlled by anomalies in SST and salinity, which can be caused locally but also via advection through anomalous surface circulation.

The Atlantic Meridional Overturning Circulation (AMOC) is a large-scale ocean circulation that contributes a large amount of about 1.3 PW (Ganachaud & Wunsch, 2003) to the meridional heat transport in the northern hemisphere. One important effect of that is the mild winter climate in Europe, which is strongly influenced by the heat transport through the North Atlantic Current and its northward extensions. Among others these currents are part of the northward surface branch of warm water within the AMOC. In the high latitudes of the North Atlantic the cold and dense North Atlantic Deep Water (NADW) is formed by deep-convection and mixing processes. In the ocean interior it flows southward, which represents the interior branch of the AMOC. The observation of the AMOC is difficult because it is a basin-wide circulation reaching from the surface to the deeper ocean levels. A method to measure the AMOC at 26°N was performed in the RAPID program which makes use of different observing systems (for details see http://www.rapid.ac.uk/rapidmoc/).

The AMOC strength is determined by several factors: Heat flux, freshwater flux, the gyre circulation, diapycnal downward mixing of heat in the high latitudes of the North Atlantic, and also Ekman induced upwelling in the Southern Ocean are suggested to influence the AMOC (Kuhlbrodt et al., 2007). The importance of heat flux anomalies for the AMOC results from its sensitivity to surface water densities in the subpolar North Atlantic. Only dense surface water can cause instability through buoyancy anomalies in the water column, which finally leads to sinking and mixing. This process is called deep-convection. The Labrador Sea, the Greenland-Iceland Norwegian (GIN) Sea, and the Irminger Sea are suggested to be key regions for deep-convection (Marshall & Schott, 1999; Pickart & Spall, 2007; Bacon et al., 2003). These regions are partly covered by the typical heat flux forcing pattern of the NAO, which justifies the relevance of the NAO phase and its buoyancy forcing for the AMOC. Another possibility by which the NAO controls the density of surface waters in the subpolar North Atlantic involves the subpolar gyre. The gyre accelerates and expands during a positive NAO phase. An increase in gyre strength could lead to positive anomalies in salt advection to the potential sinking regions (Hátún et al., 2005). Increased salinity can further increase the density and strengthen the AMOC. On the other hand, the subpolar gyre can also be affected by anomalous heat advection of the AMOC. A strong AMOC causes the gyre to warm (Roberts et al., 2013). Following geostrophy the gyre will slow down, which forms a negative feedback.

However, it was noted by Visbeck et al. (2003) that the knowledge about the response of the AMOC due to buoyancy anomalies is limited. The AMOC response to NAO forcing is furthermore not restricted to buoyancy mechanisms: Anomalies in wind stress change the Ekman transport and during a positive NAO phase this causes convergence at about 40°N. This has to result in downwelling and in a compensation by the AMOC.

The response of an ocean general circulation model to heat flux forcing obtained from the NCEP/NCAR reanalysis was investigated by Eden & Willebrand (2001). The first EOF mode of this heat flux forcing is basically representing the influence of the NAO. It can be described by a tripole pattern in the North Atlantic with a positive lobe over the subtropics and two negative lobes, one in the subpolar latitudes and one in the tropics. Large wintertime heat loss over the subpolar North Atlantic causes strong convection events in the same winter. It was shown that 2 to 3 years after these events the subpolar gyre accelerated. Furthermore, the variability of the AMOC represented by an index at 52°N was analyzed. This AMOC index increased in order to these convection events with another lag of 2 to 3 years. Finally, it was also mentioned that these responses do not change when the heat flux forcing is restricted to the Labrador Sea, which emphasizes the role of the Labrador Sea for the AMOC in their model.

An important aspect when looking at ocean modes forced by the atmosphere are the different time scales of atmosphere and ocean. The ocean is filtering the high frequency stochastic forcing of the atmosphere, and responds mainly in lower frequencies close to a red spectrum. Hasselmann (1976) postulates the stochastic climate model as a good approach for the temporal distribution of the variability in the atmosphere-ocean interaction. For instance, the low frequency response of the ocean to observed atmospheric forcing was also found in an analysis of the time-scales of North Atlantic SST variability in an ocean-only model (Latif et al., 2007; Álvarez-García et al., 2008). Two dominant variability modes were found: a quasi-decadal mode with a tripole pattern associated with an ocean-atmosphere feedback within the NAO, and a multi-decadal mode related to the multi-decadal SST forcing resulting from integrated NAO forcing, which was also related to AMOC anomalies. The attribution of certain ocean modes to atmospheric forcing becomes more difficult taking into account the different time scales. Considering dynamical processes like oceanic Rossby wave adjustments or anomalous advection with the mean ocean currents can help to reconstruct the reasons for a delayed and lower frequency response of the ocean.

Singular Spectrum Analysis of an AMOC index in the P86 control experiment of the Kiel Climate Model (KCM) revealed the existence of three modes (Park & Latif, 2012): Most of the AMOC variance is explained by a multi-centennial mode of about 300 to 400 years period. The second mode is the multi-decadal mode with a period of about 60 years. The third mode is a quasi-decadal mode of roughly 100 years period and explains least variability of these three modes. An experiment with idealized solar forcing pointed out that the pattern of the forcing is essential to excite a particular mode. The period of the forcing, however, is of minor importance. It was noted that the quasi-centennial mode is related to an anomalous meridional salinity advection, whereas the multi-centennial mode might be controlled by Southern Ocean deep-convection (Park & Latif, 2012; Martin et al., 2013). The multi-decadal mode is mainly associated with northern hemisphere heat flux anomalies, and momentum flux seems to play a minor role (Delworth & Greatbatch, 2000; Park & Latif, 2008).

In this thesis the response of the AMOC to NAO heat flux forcing is investigated. This forcing is obtained from reanalysis data. To impose observed forcing has an advantage in this case: A remarkable SST bias exists in the KCM and other coupled climate models. This could cause wrong feedbacks from the ocean to the atmosphere, which finally could have an impact on the NAO.

One goal of this analysis is to examine the effect of heat flux forcing of the NAO onto the AMOC, the mixed layer depth, and the barotropic streamfunction. This is motivated by the sensitivity of the AMOC to the buoyancy conditions in the higher latitudes of the North Atlantic, which has been identified as a key region of the climate: Freshening and warming projected for the subpolar North Atlantic can cause a slowing of the AMOC. A weakening of the AMOC is supported by model projections for the 21st century (Schmittner et al., 2005). But this anthropogenic weakening trend is relatively small compared to internal variability.

Further insight about the cause and the present state of AMOC variability modes, together with knowledge about their stability in a changing climate will help to estimate the range of possible future conditions. Thus, a second goal of this thesis is the investigation of the dominant modes of AMOC variability through Singular Spectrum Analysis. Finally, a comparison to a KCM control experiment will be made. Modes which are not present in the control experiment but in the forced experiment might be caused directly by the heat flux forcing.

This thesis is consists of three further chapters: The KCM, the experiments, and the methods are described in Chapter II. After that, the results are presented in Chapter III. It includes an analysis of dynamical relations, an investigation of dominant variability modes, and a comparison to the behavior of a control experiment. The results are summarized and discussed in Chapter IV.

II) DATA & METHODS

DATA

The Kiel Climate Model

The model results analyzed in this thesis have been derived with the Kiel Climate Model (KCM). The KCM is a coupled ocean-atmosphere-sea ice model. The oceanic component, NEMO, is an ocean-sea ice general circulation model (Madec et al., 1998). Via the OASIS3 (Valcke, 2006) it is coupled with the atmospheric general circulation model ECHAM5 (Roeckner et al., 2003). A schematic of the KCM components is shown in Figure 1. The horizontal atmospheric resolution is T31 (approximately 3.75° x 3.75°) with 19 vertical levels. In the ocean an irregular horizontal Mercator mesh based on 2° is used with the grid singularities placed over continents. The average resolution is 1.3° and the meridional resolution decreases up to about 0.5° close to the equator. The ocean depth is resolved by 31 vertical levels. Further details on the KCM are presented in Park et al. (2009).

Model experiments

In the following, the model experiments are described. A main goal of this thesis is to analyze the oceanic response to the heat flux forcing of the NAO in the KCM. Despite the effect of the NAO on further climate variables, this experiment is only driven by the heat flux pattern associated with the NAO. In the following, this experiment is labeled NAO-HF. To derive the heat flux forcing, the Hurrell station-based NAO index (Figure 2) obtained from sea level pressure differences between the subpolar Stykkisholmur in Iceland and the subtropical Lisbon in Portugal was used. Regression patterns of NCEP/NCAR reanalysis (Kalnay et al., 1996) heat flux data onto the monthly station-based Hurrell NAO index (Hurrell, 1995) were obtained using the observation period 1958-2000. These patterns were multiplied by the NAO index of the years 1865 to 2010 yielding the forcing of this experiment. However, the following analyzes are restricted to the period from 1900 to 2010. Only the mean of the 9 ensemble members will be used.

The results were compared with the variability in an unforced control experiment (experiment id: W03). Its boundary forcing are the present-day values, e.g. CO2=348 ppm. It is 1000 years long starting from the Levitus climatology (Levitus et al., 1998). It is noteworthy that the NAO-HF experiments were initialized from the years 695, 700, and 705 of the W03 control

integration. To avoid larger effects of model spin-up only the years 300 to 999 were used in this thesis.

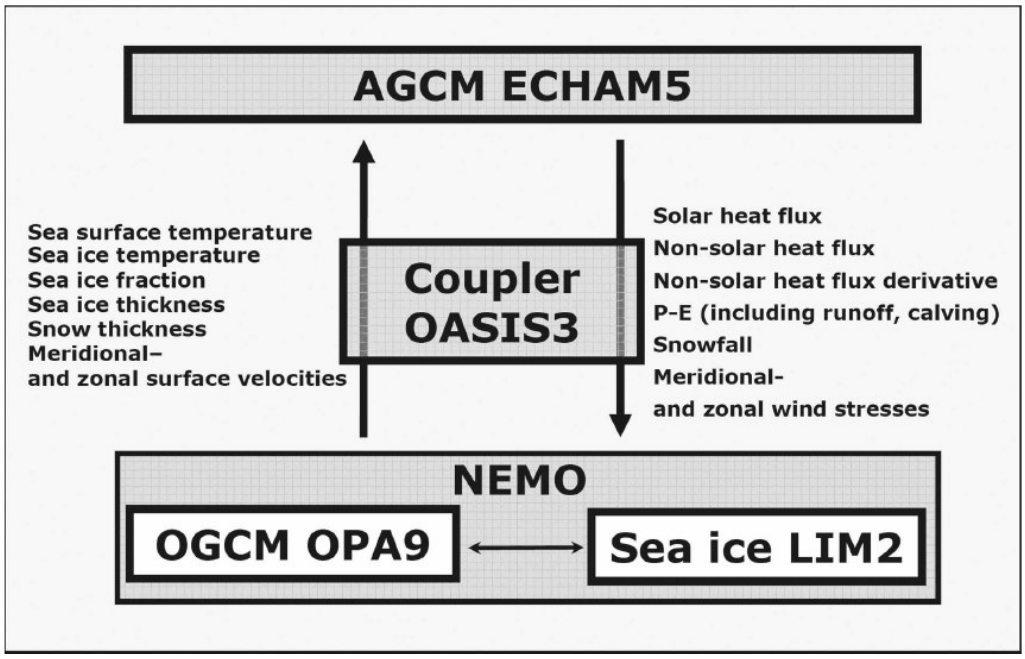

Figure 1: Components of the Kiel Climate Model (from: Park et al., 2009)

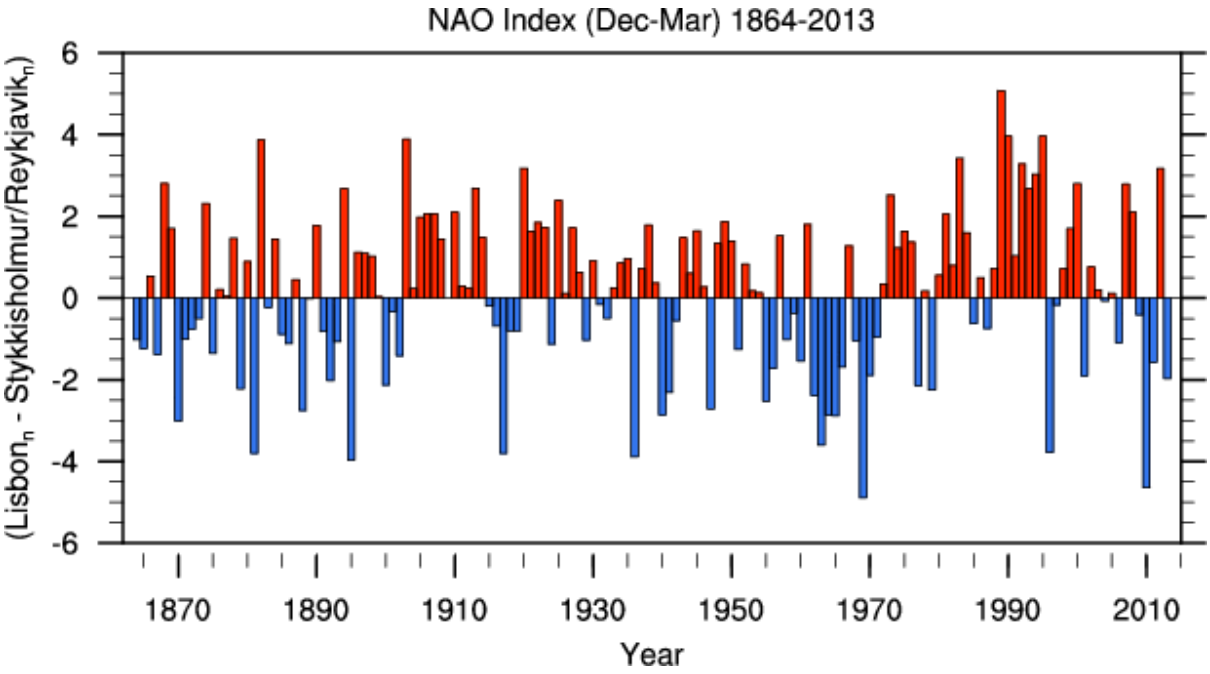

Figure 2: Hurrell station-based NAO index obtained from winter (December-March) sea level pressure (from: https://climatedataguide.ucar.edu/climate-data/hurrell-north-atlantic-oscillation-nao-index-station-based)

Analyzed variables

The strength of the AMOC index at 30°N is defined by the maximum in the meridional overturning streamfunction at 30°N. The resulting overturning maximum of 30°N is located at a depth of 612 m in the NAO-HF experiment and only slightly deeper in the control experiment.

Further KCM outputs analyzed in this thesis are: ocean heat content of the upper 1000 m, barotropic streamfunction, and mixed layer depth. For these variables an index is defined by area-averaging over 50°-15°W and 45°-62°N, which roughly represents the location of the subpolar gyre in the North Atlantic.

METHODS

All results are based on detrended annual anomalies. All regressions are done onto normalized variables, yielding values in the unit of the regressed variable.

NAO index

In the control experiment the NAO index is not prescribed but calculated from the model outputs. For a better comparison, both a station-based and a principal component (PC)-based NAO index were derived from the simulated sea level pressure. The steps are based on the method of Hurrell (1995). First of all, the sea level pressure was averaged for each year from December to March. Then, for each grid point the mean and the trend were subtracted and they were normalized by their standard deviation. The normalization is commonly done to avoid that the NAO index is stronger influenced by the subpolar low pressure center, which has a larger variability than the high pressure center. Finally, the station-based index is derived from the difference between two stations, one placed in the low pressure center and one in the high pressure center. Here, the closest grid points to the stations Stykkisholmur (65.07°N, 22.72°W) and Lisbon (38.72°N, 9.17°W) were chosen. For the purpose of comparing also the pattern of NAO variability a PC-based NAO index was derived. After the step of normalization, a PC analysis was carried out, yielding a spatial pattern for each mode and a corresponding time series.

Singular Spectrum Analysis

The dominant modes are derived with Singular Spectrum Analysis (SSA). With this method variability modes of different periods can be filtered out and their reconstructions can be derived (e.g., Ghil et al., 2002). For the SSA analysis in this thesis a toolkit was used which is described in Dettinger et al. (1995) and Ghil et al. (2002). Variables defined on a vector space can be analyzed by extending SSA to MSSA (Multiple Singular Spectrum Analysis), but in this thesis the results were obtained only from variable indices, and therefore, SSA. The main steps of SSA can be described as follows:

From a spatially one-dimensional time series x_t of length N [$t=1,\ldots,N$] one derives its lagged versions up to a maximum lag equal to $M-1$, with M called the window length. Starting at a lag of zero one gets M shifted vectors of length $N-M+1$. These vectors can be written into a matrix:

$$X_{lag\text{-}matrix} = \begin{bmatrix} x_1 & \cdots & x_{N-M+1} \\ \vdots & \ddots & \vdots \\ x_{M-1} & \cdots & x_N \end{bmatrix}. \qquad (1)$$

From this matrix the covariance matrix has to be estimated. This is done with the estimation method of Vautard & Ghil (1989) which involves the conversion of the data into a Toeplitz matrix with constant diagonals. Finally, the eigenvalues λ_k of the covariance matrix are obtained. The eigenvalues are put into a decreasing order according to their explained variance regarding the time series x_t. For all eigenvalue λ_k corresponding eigenvectors ρ_k are obtained. The eigenvectors are sometimes called EOFs (referring to Empirical Orthogonal Functions). Now, the time series x_t can be projected onto each particular eigenvector ρ_k:

$$A_k(t) = \sum_{j=1}^{M} x(t+j-1)\ \rho_k(j)\ . \qquad (2)$$

These projections A_k are called principal components (PCs) in this thesis. Finally, one can reconstruct the time series based on a single or a set K of particular PCs:

$$R_K(t) = \frac{1}{M_t} \sum_{k \in K} \sum_{j=L_t}^{U_t} A_k(t-j+1)\ \rho_k(j). \qquad (3)$$

The normalization factor M_t and also the bounds of the summation U_t and L_t are dependent on t. Further details on those values are given in Ghil & Vautard (1991) and Vautard et al. (1992). Hereafter, a reconstructed time series R_K is obtained that displays only the variability contribution of a single or a set of modes.

When applying SSA one must consider that an oscillatory mode of variability is represented by a pair of eigenvalues that are approximately of the same size. Further pairing criteria are that their PCs oscillate with roughly the same period and with a phase shift of about $\frac{\pi}{2}$ (e.g., Jolliffe, 2002). Significance of the modes against the hypothesis of red noise is done with a Monte Carlo test as described by Allen and Robertson (1996).

In the NAO-HF experiment the window length in the SSA was chosen to be 56 years (approximately half the length of the time series). As a test of robustness the window length was also set to 41, 46, 51, and 61 years without notable changes in the results. For the W03 control experiment results are shown for a window length of 100 years.

III) RESULTS

DYNAMICAL MECHANISMS

In the NAO-HF experiment the forcing is the heat flux anomaly associated with the NAO index (Figure 3a). The regression of heat flux onto the NAO index is shown in Figure 3b. It consists of a tripole pattern with a strong negative heat flux in the subpolar North Atlantic extending from the Labrador Sea in the west to Iceland in the east. During a positive NAO phase the areas of negative values indicate an energy loss for the ocean and thus a cooling. The most negative value is approximately -9 Wm^{-2} and is located in the Labrador Sea. Positive heat flux is found in the west of the North Atlantic from 30° to 45°N. With a maximum of about 3 Wm^{-2} it is weaker than the subpolar center. In the east of the tropical North Atlantic there is a further region of ocean cooling during a positive NAO index but it is much smaller and also relatively weak compared to the other tripole centers. Furthermore, there is some negative heat flux in the Greenland Sea and some positive heat flux aside of that towards the Norwegian Sea. In the western and middle North Atlantic this pattern is increasing the meridional temperature gradient between the subpolar and the subtropical latitudes of the North Atlantic. Furthermore, the cooling in the subpolar region will tend to produce anomalously thick mixed layers by decreasing the stability of the water column.

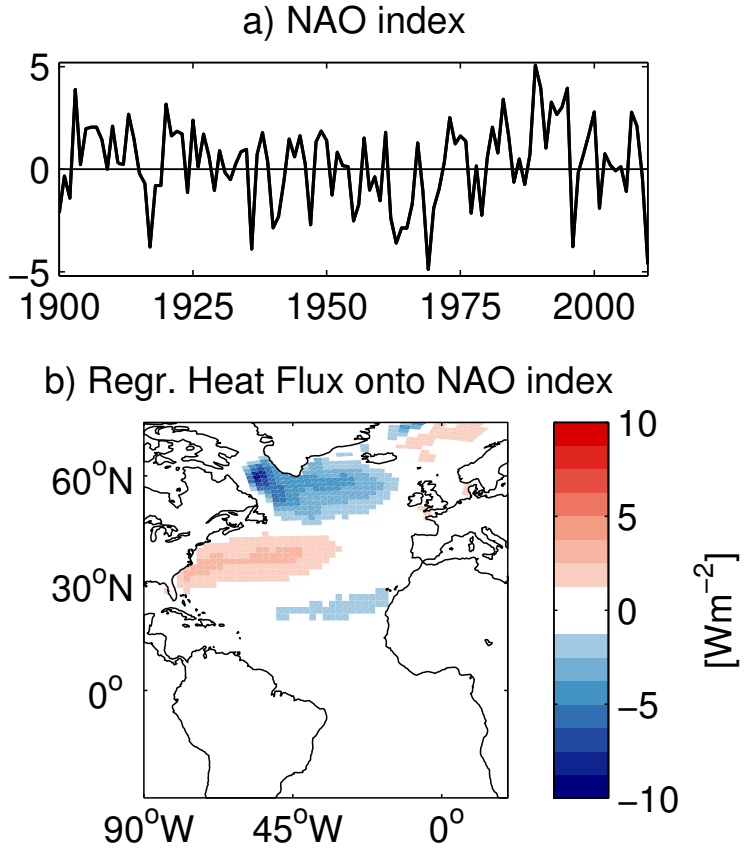

Figure 3: The NAO index (a) and the regression of heat flux onto the normalized NAO index (b). Negative values indicate a heat loss for the ocean.

The same pattern is also found in the regression of the heat flux onto the AMOC 30°N index (Figure 4), especially, when the heat flux leads the AMOC by 4 to 6 years. At other time lags between 2 and 14 years the pattern is similar but weaker. No immediate response to the forcing (lag = 0 y) of the AMOC can be found. Apparently, the AMOC at 30°N is influenced by the heat flux forcing but it takes some years until it becomes affected.

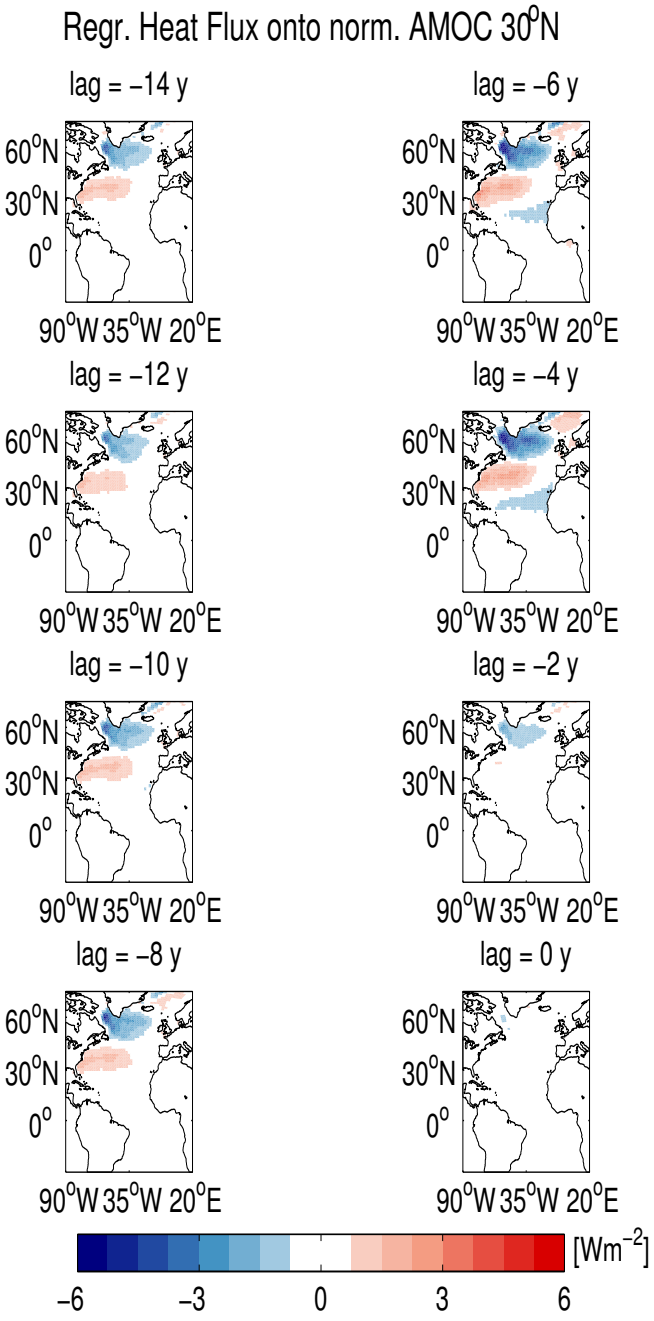

Figure 4: Regression of heat flux onto the normalized AMOC 30°N index for different lags. Negative lags indicate that heat flux is leading.

The mean states over the period 1900-2010 of the NAO-HF experiment are shown in Figure 5. The AMOC represented by the meridional overturning streamfunction (Figure 5a) has a positive cell in the upper ocean reaching down to about 2500 m and below that a negative cell expanding to the bottom. The maximum of the positive cell is about 15 Sv (Sv = 10^6 m^3s^{-1}) and therefore stronger than the maximum of the negative cell reaching only 7 Sv. The positive streamfunction indicates a northward flow at the surface and a southward flow in the depth of around 1000 to 2000 m. The AMOC index will be defined as the maximum in the streamfunction at 30°N and its strength varies between 9.8 and 16.0 Sv.

The mean state of the ocean heat content of the upper 1000 m (Figure 5b) has a maximum of 71 GJm^{-2} located in the west of the subtropical North Atlantic. This is the region from which the Gulf Stream starts to flow northeastwards. High latitudes and areas with ocean depths lower than 1000 m have, due to low temperatures and to vertical integration respectively, the lowest mean heat content.

The mean of mixed layer depth (Figure 5c) is largest in a spot located at around 55°N and 20° to 40°W. There it goes down to more than 700 m. Around 400 to 500 m are reached in two regions: south of Iceland extending to Scotland and also at the border between the Greenland Sea and the Norwegian Sea. In general, mixed layer depth is large in areas where oceanic convection takes place. Note that for this process the winter mixed layer depth is important and this reaches even deeper than the annual mean. However, the pattern of winter and annual mean mixed layer depth is very similar. An important result is that there is no convection in the Labrador Sea. This is a bias of the KCM, in which the Labrador Sea is largely covered with sea ice.

Finally, the barotropic streamfunction is shown in its mean state (Figure 5d). Its most obvious patterns in the North Atlantic are the subpolar and the subtropical surface gyres. The subpolar gyre is negative in its mean state. This means that the subpolar gyre circulates anti-clockwise. Its most negative value is about -28 Sv. The subtropical gyre, however, is positive and circulates clockwise. In the tropics the streamfunction is not as pronounced. The subtropical gyre in the South Atlantic is located south of 20°S and is therefore not fully included in the chosen map.

The subpolar gyre in the North Atlantic plays an important role in this study of ocean response to NAO heat flux forcing. Therefore, a rectangular box around the subpolar gyre

(see box in Figure 5d) is chosen to serve as an averaging area for subpolar gyre indices which will be investigated.

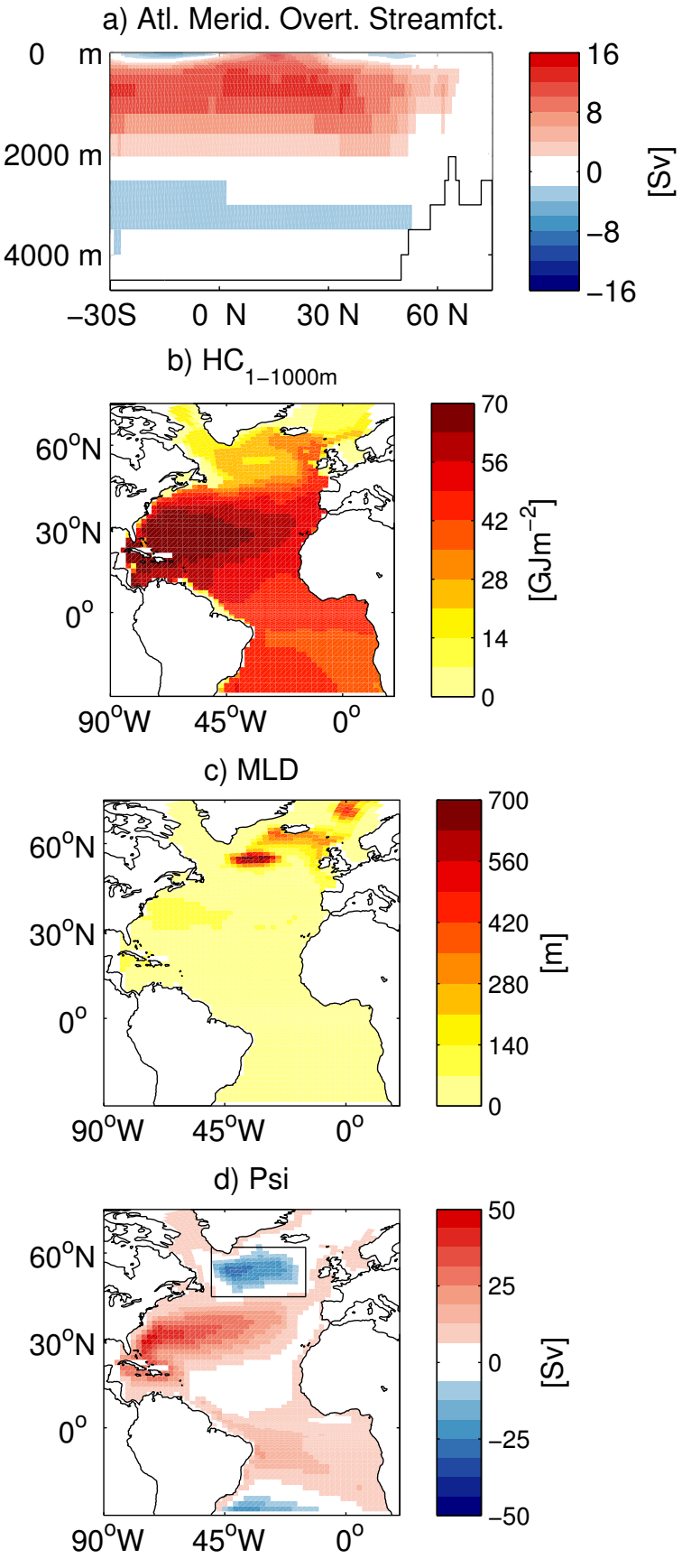

Figure 5: Mean states (1900-2010) of a) Atlantic meridional overturning streamfunction, b) Ocean Heat Content in the upper 1000 m, c) Mixed layer depth, and d) Barotropic Streamfunction. The box in (d) indicates the averaging area used for the subpolar gyre region.

In the following, only annual mean deviations from the mean states will be analyzed.

The 11-year running mean time series of the different indices are shown in Figure 6. The major positive phases of the NAO index are the periods 1900 to 1934 and 1975 to 2010. From 1935 to 1974 it is mainly negative interrupted by a minor positive phase from 1945 to 1950. For the barotropic streamfunction a subpolar gyre index (Figure 6b) was defined by averaging over the box shown in Figure 5d and by multiplying the result by -1. Also the mixed layer depth index (Figure 6c) is an average of the subpolar gyre box. Positive values of this index indicate anomalously deep mixed layers. Both of these subpolar gyre indices and also the AMOC 30°N index (Figure 6d) display a similar behavior matching roughly the time series of the NAO index: First, there is a drift towards positive anomalies. Then the response becomes negative and returns finally to positive values. Except of the time before 1934, the variables seem to follow the NAO index. However, the time lag in the response to the NAO index is different. The mixed layer depth responds rapidly without any lag in time, the subpolar gyre strength is following soon after 1 to 2 years, and the AMOC 30° index lags by about 3 to 14 years. Moreover, the AMOC response to the NAO seems to propagate from around 50°N to the south which is reflected by the AMOC time series of different latitude (Figure A2, appendix).

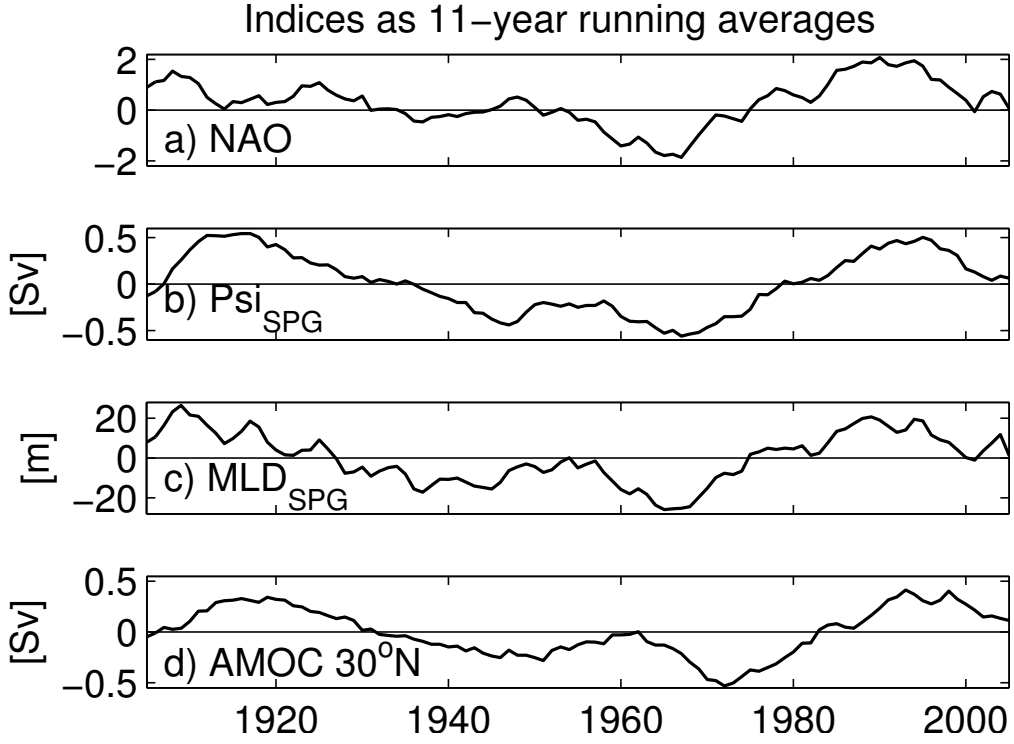

Figure 6: Time series as 11-year running means of a) the NAO index, b) the subpolar gyre strength, c) the mixed layer depth in the subpolar gyre, d) the AMOC index at 30°N

The behavior of these variables is further analyzed using unfiltered annual variables. Cross-correlations to the NAO index are shown in Figure 7a-c. The subpolar gyre strength is most correlated for a lag of 1 year yielding a correlation coefficient of 0.37. However, all correlations with lags of 0 to 10 years are significant. The mixed layer correlation coefficient has a distinct and significant maximum of 0.75 at zero lag, which indicates an immediate response to the NAO. Largest correlations of NAO and the AMOC 30°N index are found in a wider range of lags: from 3 to 10 and from 12 to 14 years with a maximum of 0.4 at a lag of 13 years.

Further cross-correlations with the AMOC were analyzed: First, the cross-correlation between the mixed layer depth in the subpolar gyre and the AMOC 30°N index (Figure 8a). Mixed layer depth leads the AMOC index by 2 to 14 years with a maximum correlation coefficient of 0.38 at 6 years lag. Second, a maximum in correlation of 0.54 is found for the subpolar gyre strength leading the AMOC 30°N by 5 years (Figure 8b).

In addition, these cross-correlations were also computed for the AMOC index at 45°N. It responds earlier to the heat flux forcing which supports that the signal propagates from the subpolar North Atlantic to the south. The correlation of the AMOC at 45°N to the NAO index and the mixed layer depth is largest at a time lag of 3 years. The subpolar gyre strength is responding simultaneously with the AMOC at 45°N (Figures A3 & A4, appendix).

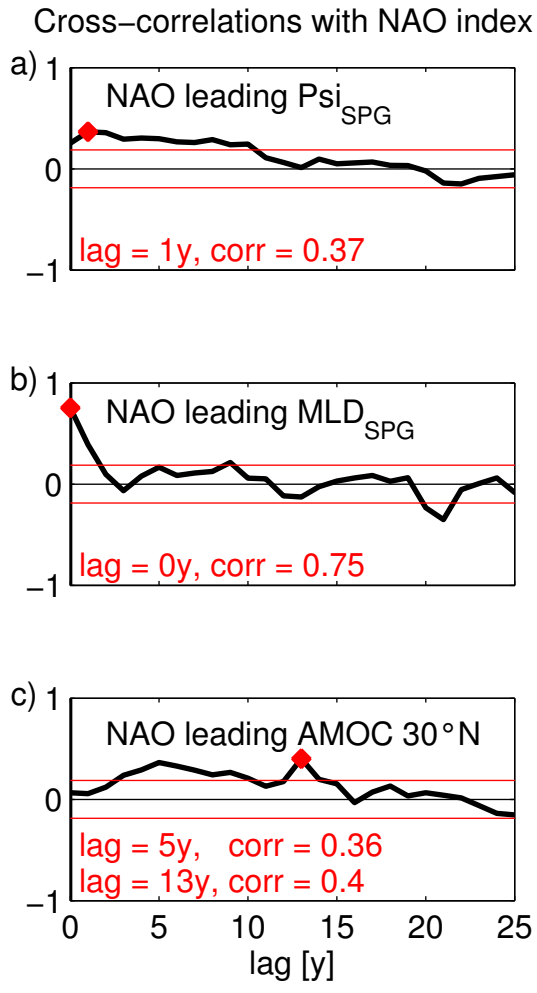

Figure 7: Cross-correlation between the NAO index and a) the subpolar gyre strength, b) the mixed layer depth of the subpolar gyre, and c) the AMOC 30°N index. The red horizontal lines indicate the 95%-confidence intervals.

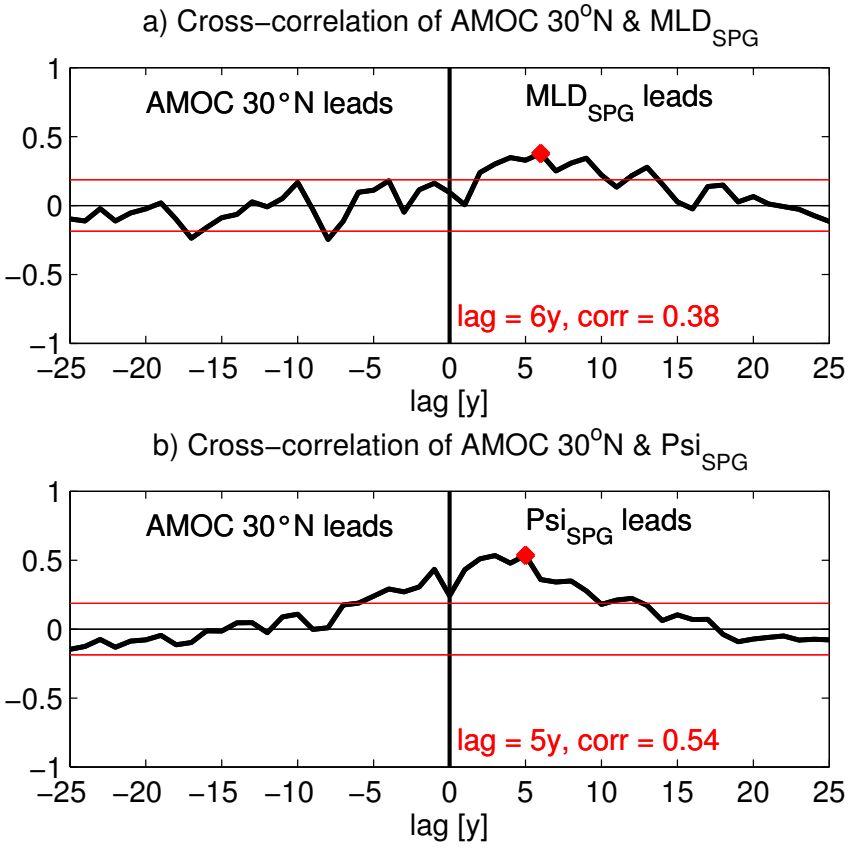

Figure 8: Cross-correlation between the AMOC 30°N index and the mixed layer depth of the subpolar gyre (a) and the AMOC 30°N index and the subpolar gyre strength (b). The red horizontal lines indicate the 95%-confidence intervals.

The regression of the Atlantic meridional overturning streamfunction onto the NAO index was calculated for different lags (Figure 9). The green dot indicates the location of the AMOC 30°N index. At zero lag no correlation is found in this location, which agrees with Figure 4 (lag = 0 y). In the streamfunction regressions, the 30°N index is placed below a smaller spot of negative regressions confined to the surface and above a larger region of positive regression with its center farther in the north. The latter region is expanding from the surface to about 3000 m depth. It is also the major response signal of the overturning considering also the lagged regressions. With increasing lag in time this positive response to the NAO index and expands to the south. The lags were chosen on the basis of Figure 7c: A first maximum of correlation is reached at a lag of 5 years, turning back below the 95%-confidence limit at 11 years, and reaching a further maximum at 13 years. Now, comparing the corresponding pattern (Figure 9), this development can be explained by the fact that the center of negative regression is located farther north and also deeper than the location of the AMOC 30°N index.

For further insight into the important response processes, the mixed layer depth, and the barotropic streamfunction were regressed onto the NAO index (Figure 10). The immediate response of mixed layer depth (Figure 10a) is confined to the area of the deepest mean state values (cf. Figure 5c). In the case of a positive NAO phase the subpolar gyre region in the

North Atlantic cools and the mixed layer depth becomes thicker by up to 120 m. There is nearly no response in the Labrador Sea. The response of the barotropic streamfunction is shown for the case that the NAO index is leading by 1 year (Figure 10b). Other lags reveal similar but weaker patterns. Over the subpolar gyre there is a negative and over the subtropical gyre there is a positive anomaly during a positive NAO phase. Note that the different signs of these gyre anomalies must be compared to the signs of their mean state (Figure 5d). This means that the subpolar and the subtropical gyre accelerate during a positive NAO index. Though, this effect is more pronounced for the subpolar gyre.

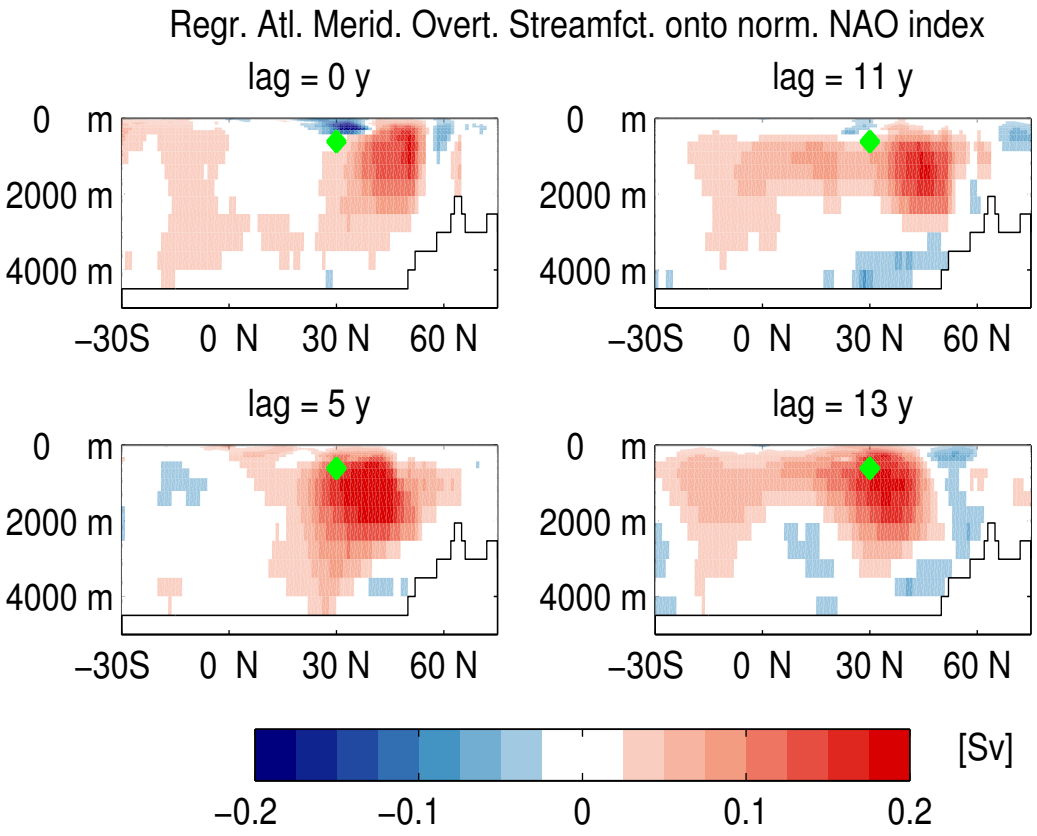

Figure 9: Regression of the Atlantic meridional overturning streamfunction onto the normalized NAO index for different lags. Positive lags indicate that the NAO leads. The green dot indicates where the AMOC 30°N index is located.

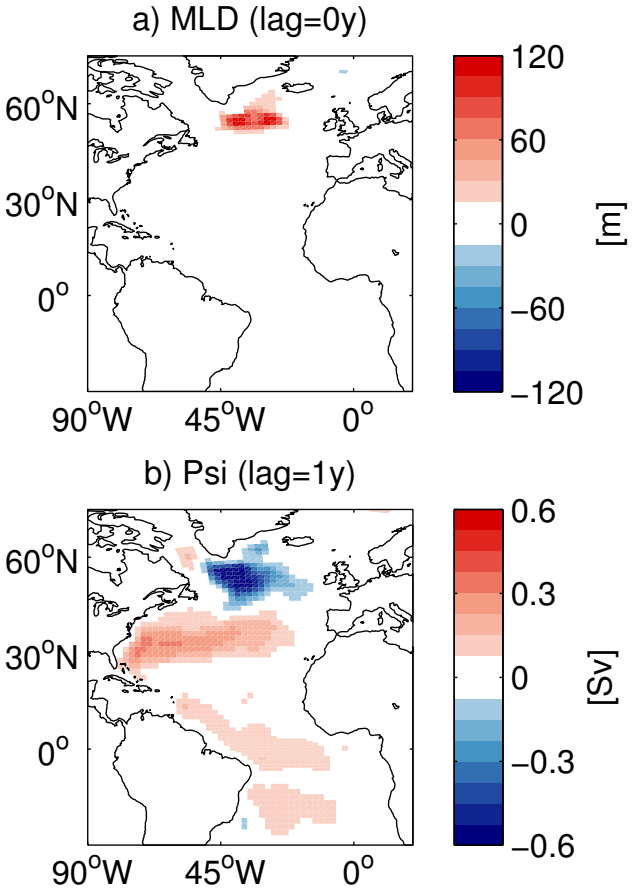

Figure 10: Regressions of a) mixed layer depth [without any lag], b) barotropic streamfunction onto the normalized NAO index. Positive lags indicate that the NAO leads.

DOMINANT MODES

In the following, the dominant modes of variability will be analyzed for the NAO-HF experiment. The forcing NAO index is an atmospheric parameter, but its power spectrum is not white but slightly red (Figure 11). Peaks in the NAO power spectrum are located at multi-decadal and interannual to decadal periods. These peaks are significant against red noise on a 95%- and some even on a 99%-confidence level.

Singular Spectrum Analysis (SSA) is used to identify the dominant modes of variability and to build their time series reconstructions. Using a window length of 56 years the SSA of the NAO index derives eigenvalues with explained variance as shown in Figure 12a. The first two eigenvalues explain together 14% of the NAO variability. The third and the fourth eigenvalue explain in sum 11%. For the PCs 1 and 2 (Figure 12b, upper panel) it is not entirely clear whether they form an oscillatory pair. The PCs are not clearly having the same period and a phase shift of roughly 90°. This is also a result of the shortness of the remaining PC time

period of 56 years compared to the possible oscillation period of about 58 years. Though, the conditions for an oscillatory pair are more clearly fulfilled by the pair 3, 4. Its oscillation period is 8 years. Only the mode of 8 years is significant against red noise at a confidence level of 95% (see Figure A8, appendix). The resulting time series reconstructions are shown in Figure 12c. Obviously, the reconstruction of the PC pair 1, 2 with a period of around 58 years (red line) is mainly explaining the negative NAO phase in the in the 1960s and the following strong positive NAO phase in the 1990s. The PC pair 3, 4 with the period of 8 years (bluen line) explains the interannual variability of the NAO index. Combining the first four components about 26 % of the variability can be explained.

The regression of only the 58 year mode reconstruction of the NAO index onto the normalized field of the meridional overturning streamfunction (Figure A15, appendix) is quite similar to the pattern that is obtained when using the full NAO index (Figure 9). The regression of the 8 year mode reconstruction (Figure A16, appendix) is much weaker of a different pattern. This suggests that the AMOC variability is mainly influenced by the low frequency 58 year mode of the NAO.

The first two eigenvalues of the AMOC 30°N SSA explain together 34%, the third and the fourth eigenvalue only 17 % (Figure 13a). The first four eigenvalues add up to 51% explained variance which is relatively high compared to the case of the NAO index, where the first four eigenvalues explain only 26%. For the pair 1, 2 it is again not so clear as for the pair 3, 4 if they form an oscillatory pair. But again the PC length of 56 year is very short compared to a period of about 93 years in the pair 1, 2 (Figure 13b,c). The pair 3, 4 has a period of about 36 years. Nevertheless, the 93 year mode is significant against red noise at a confidence level of 95%, whereas the 36 year mode is not (Figure A9, appendix).

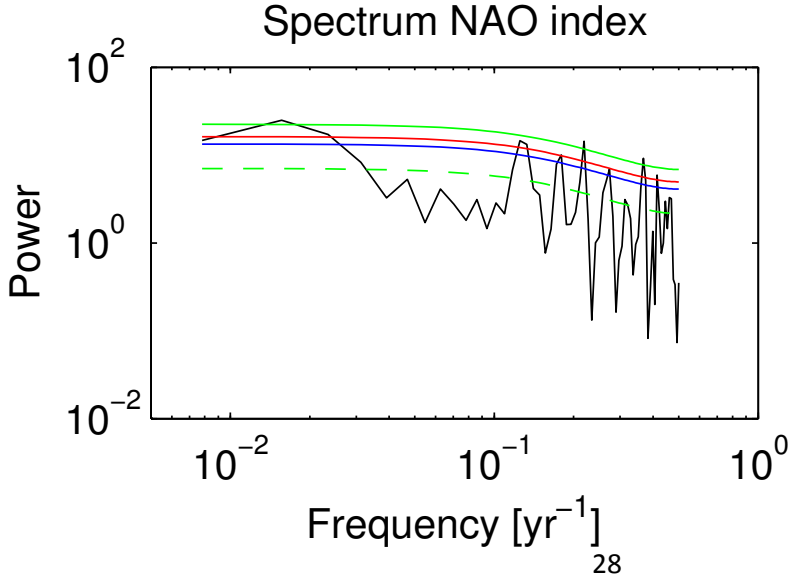

Figure 11: Power spectrum of the NAO index. The green dashed line indicates the spectrum of an autoregressive process, the blue line its 90%-, the red line its 95%-, and the green solid line its 99%-confidence limit.

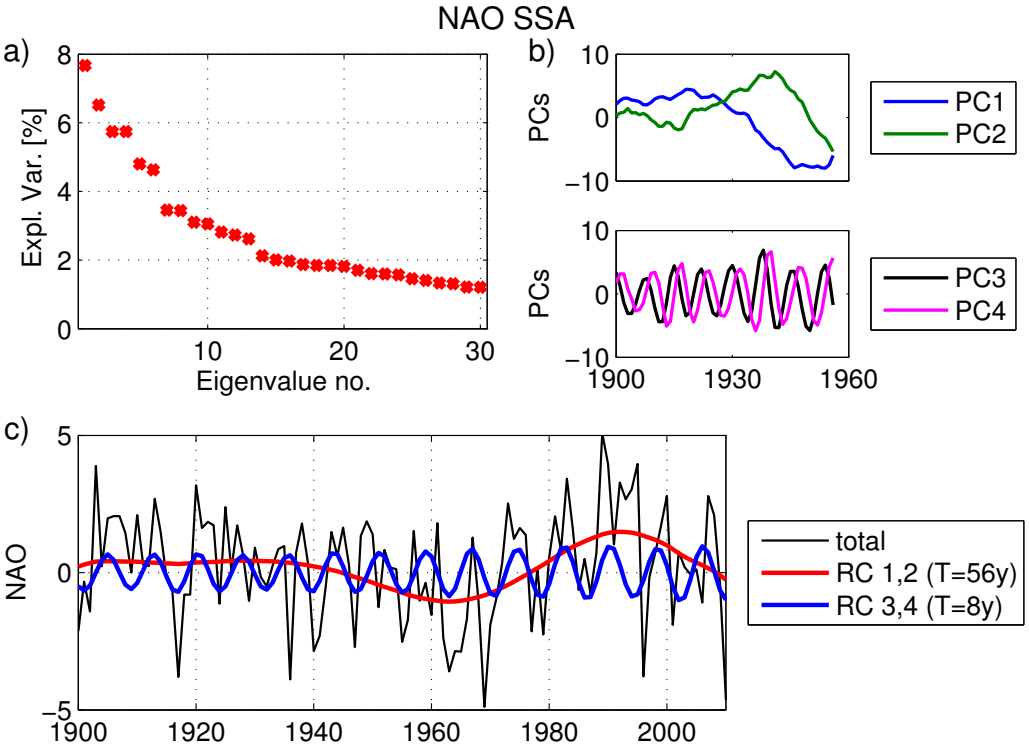

Figure 12: SSA results for the NAO index with a window length of 56 years. Shown are the percentages of explained variance (a), and for the leading modes also the principal-components (b) and the time series reconstruction (c).

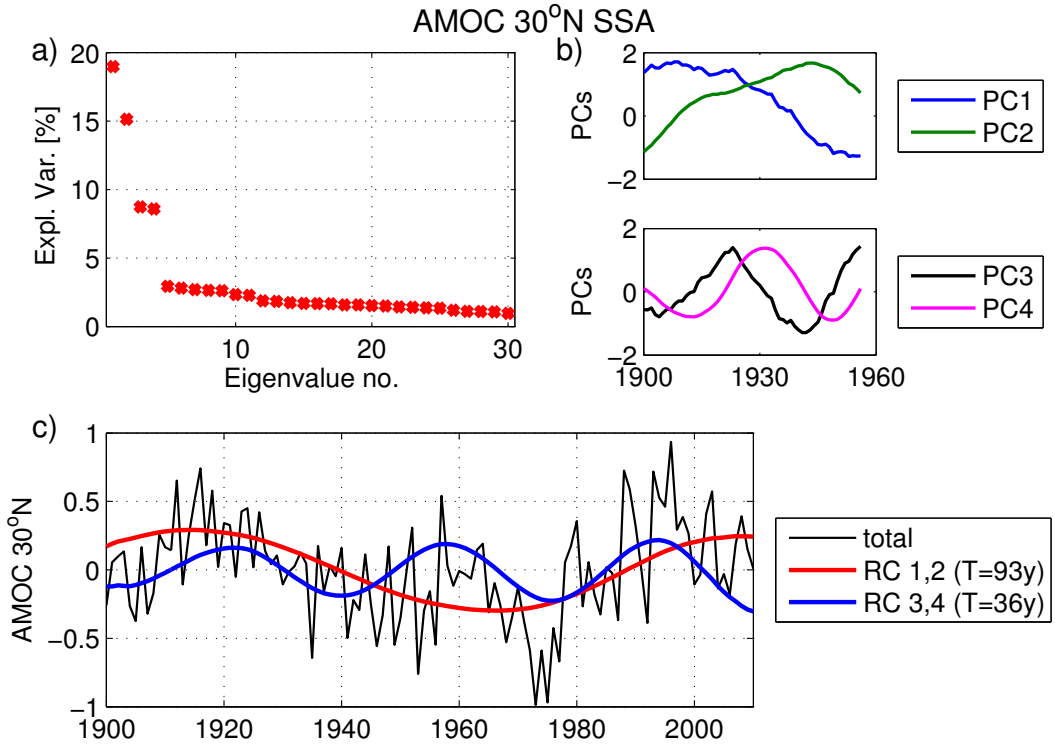

Figure 13: SSA results for the AMOC 30°N index with a window length of 56 years. Shown are the percentages of explained variance (a), and for the leading modes also the principal-components (b) and the time series reconstruction (c).

It was also tested how the results change when the AMOC index at 45°N is used (Figure A12, appendix). A long mode of 87 years and a shorter one of 36 years were identified. Thus, only the long mode has a slightly shorter period compared to the AMOC at 30°N. The period of the short mode is exactly the same for both indices.

For the mixed layer depth (Figure 14) the short 8 year period, which was already dominant for the NAO index, is the leading oscillatory pair. This mode is explaining 16% of the total variance. The following eigenvalues are not forming pairs based on the different behavior of their PCs (not shown). Nevertheless, the reconstruction based on the third eigenvalue explaining 7% is also shown. It behaves similar to an oscillation with a period of roughly 84 years. The first two eigenvalues of the SSA for the subpolar gyre strength (Figure 15) explain 37% of the total variance. If they form an oscillatory pair is not clear, also due to their long period of 80 years compared to the total time series length of 111 years.

Normalized reconstructions of all variables are shown in Figure 16. Correlations between these time series are listed in Table 1. Among the shorter modes (Figure 16a) there is an 8 year period in the NAO index but also in the mixed layer depth index. These two reconstructed time series have the highest correlation when the NAO leads by 1 year (Table 1). The period of the AMOC mode of 36 years matches with no other time series. The modes of longer periods (Figure 16b) are all significantly correlated (Table 1). The highest correlation of 0.99 is obtained when the 84 year component of the mixed layer depth leads the long AMOC mode by 10 years. However, the length of the time series is short compared to their oscillation periods and the NAO mode of 58 years does not have a stable oscillation before the end of the 1930s. Around the 1960s the retreat from the negative maximum in the subpolar gyre strength and the low frequency mixed layer depth component starts earlier than in the NAO 58 year mode (Figure 16b). But as the NAO is prescribed here, this cannot be caused by a process where the ocean leads the atmosphere. Despite the conditions in this model such a process might have caused the low frequency variability in the NAO reanalysis data. Finally, one can conclude that the longer AMOC mode of 93 years correlates better with modes of other variables than the mode of 36 years.

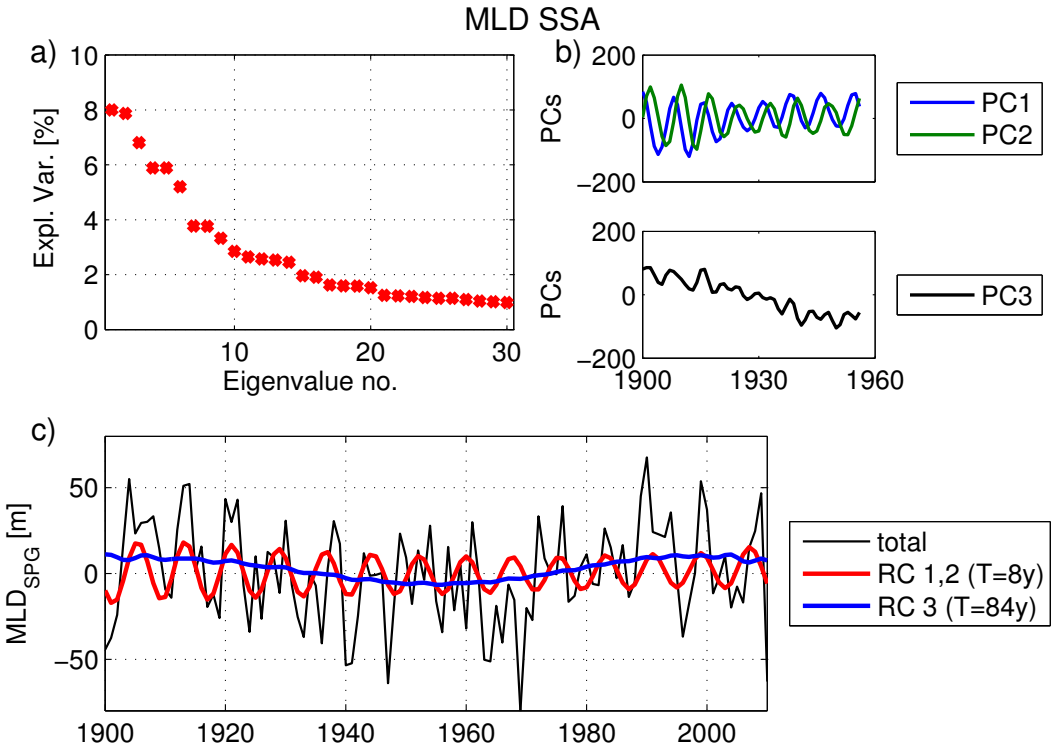

Figure 14: SSA results for the mixed layer depth averaged over the subpolar gyre with a window length of 56 years. Shown are the percentages of explained variance (a), and for the leading modes also the principal-components (b) and the time series reconstruction (c).

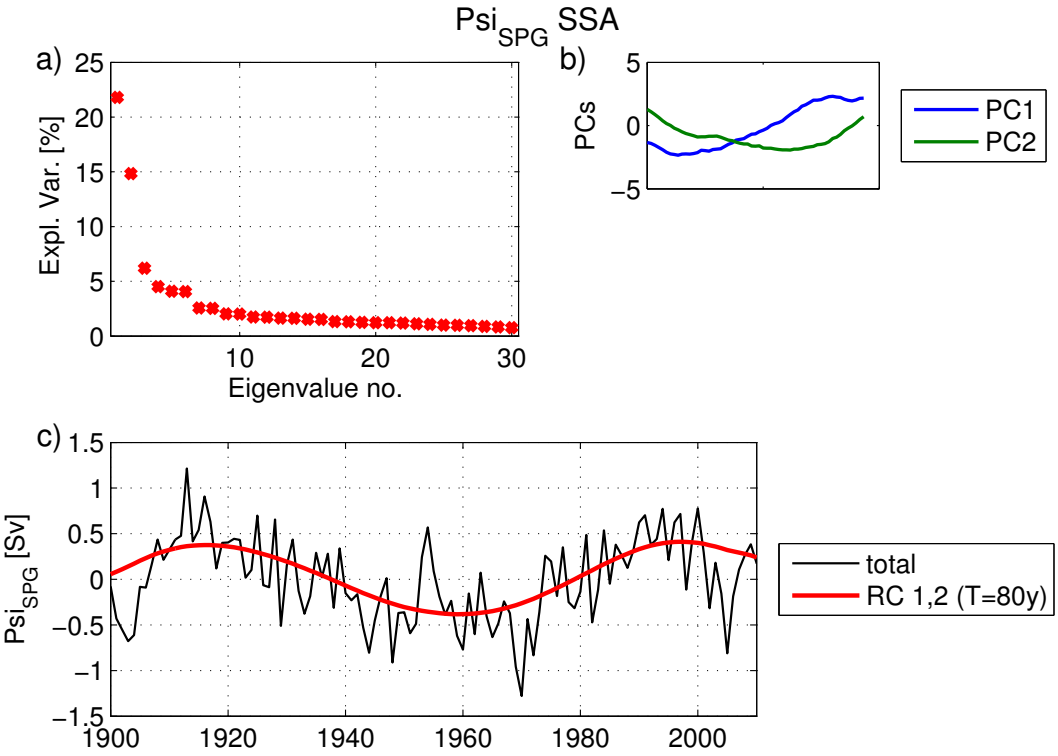

Figure 15: SSA results for the subpolar gyre strength with a window length of 56 years. Shown are the percentages of explained variance (a), and for the leading modes also the principal-components (b) and the time series reconstruction (c).

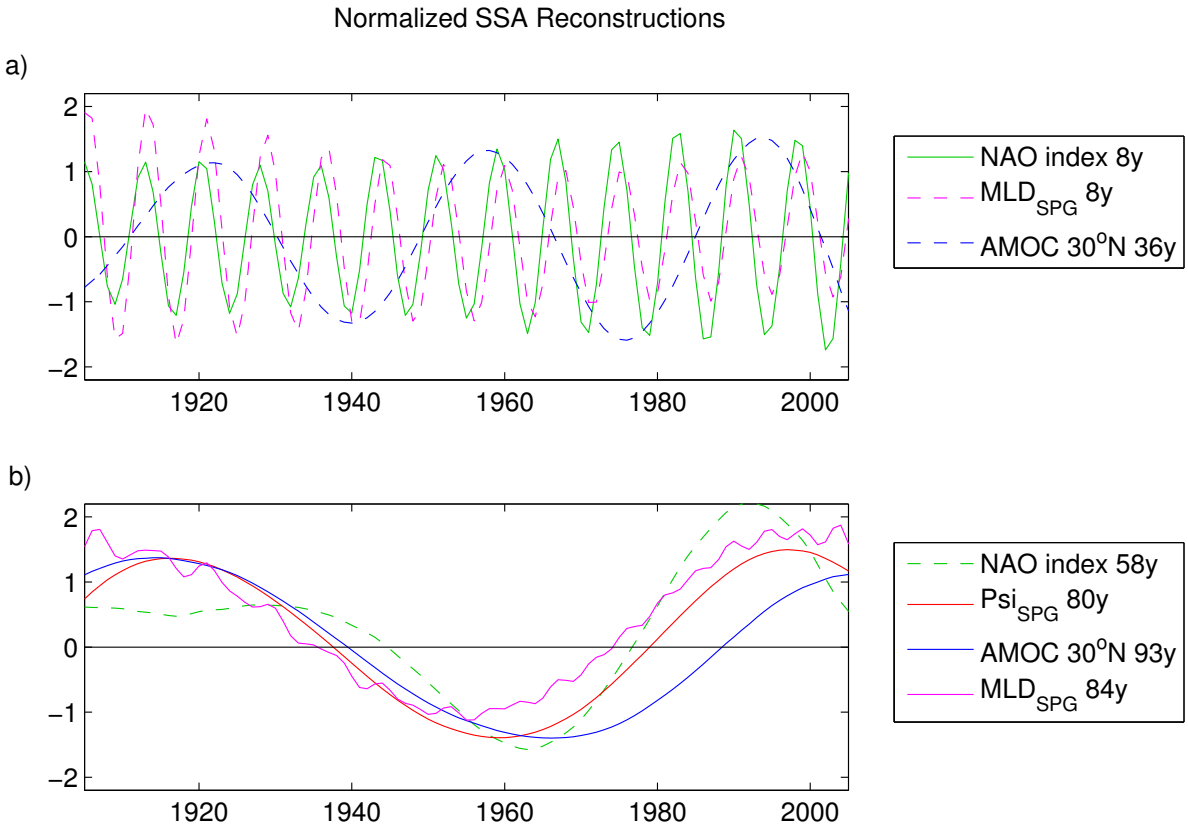

Figure 16: Normalized SSA time series reconstructions of a) the 8 year mode of the NAO index, and the mixed layer depth 8 year mode, and the AMOC 30°N 36 year mode, and b) the NAO index 58 year mode, the subpolar gyre strength 80 year mode, and the AMOC 30°N index 93 year mode, and the mixed layer depth 84 year component.

In the following, regressions onto the two different AMOC modes were computed to investigate whether different dynamical reasons for the two modes, one of 93 years and one of 36 years period, can be identified.

First of all, regressions of the Atlantic meridional overturning streamfunction onto the reconstructions of the AMOC 30°N index for different time lags were computed (Figure 17 & 18). In these figures the lags for the long oscillation of the 93 year mode (Figure 17) were chosen to cover a larger time period than for the 36 year mode (Figure 18). Despite the different time scales, the AMOC response of both is dominant at around 45°N and at a depth of 1000 to 2000 m, which is again farther north and deeper than the location of the AMOC 30°N index (green dots in Figures 17 and 18). The main pattern is similar, but a difference is that the pattern of the 93 year mode response has a notable vertical signal propagation down to about 3500 m depth together with a southward component. The signal in the 36 year mode

response however, has mainly a horizontal signal propagation reaching even 20°S with nearly no vertical component. Moreover, one can see that the main signal evolving at around 45°N appears already 12 years earlier than in the 93 year mode of the AMOC 30°N index (Figure 17, lag = -12 y) and 5 years earlier than in the 36 year mode (Figure 18, lag = -5 y).

Correlation	NAO 8 y	NAO 58 y	Psi_SPG 80 y	MLD_SPG 8 y	MLD_SPG 84 y	AMOC 30°N 93 y	AMOC 30°N 36 y
NAO 8 y	-	0.02	0.00	**0.75 [0.90 for NAO leading by 1 year]**	-0.02	-0.02	0.02
NAO 58 y	0.02	**-**	**0.85 [0.86 for NAO leading by 2 years]**	0,08	**0.79 [0.80 for MLD_SPG leading by 2 years]**	**0.62 [0.79 for NAO leading by 8 years]**	0.14
Psi_SPG 80 y	0.00	**0.85 [0.86 for NAO leading by 2 years]**	-	0.11	**0.93 [0.97 for MLD_SPG leading by 4 years]**	**0.89 [0.95 for Psi_SPG leading by 6 years]**	0.13
MLD_SPG 8 y	**0.75 [0.90 for NAO leading by 1 year]**	0.08	0.11	-	0.11	0.08	-0.01
MLD_SPG 84 y	-0.02	**0.79 [0.80 for MLD_SPG leading by 2 years]**	**0.93 [0.97 for MLD_SPG leading by 4 years]**	0.11	-	**0.80 [0.99 for MLD_SPG leading by 10 years]**	0.05
AMOC 30°N 93 y	-0.02	**0.62 [0.79 for NAO leading by 8 years]**	**0.89 [0.95 for Psi_SPG leading by 6 years]**	0.08	**0.80 [0.99 for MLD_SPG leading by 10 years]**	-	0.06
AMOC 30°N 36 y	0.02	0.14	0.13	-0.01	0.05	0.06	-

Table 1: Correlation between the different SSA time series reconstructions. Bold numbers indicate significance at 95%-confidence.

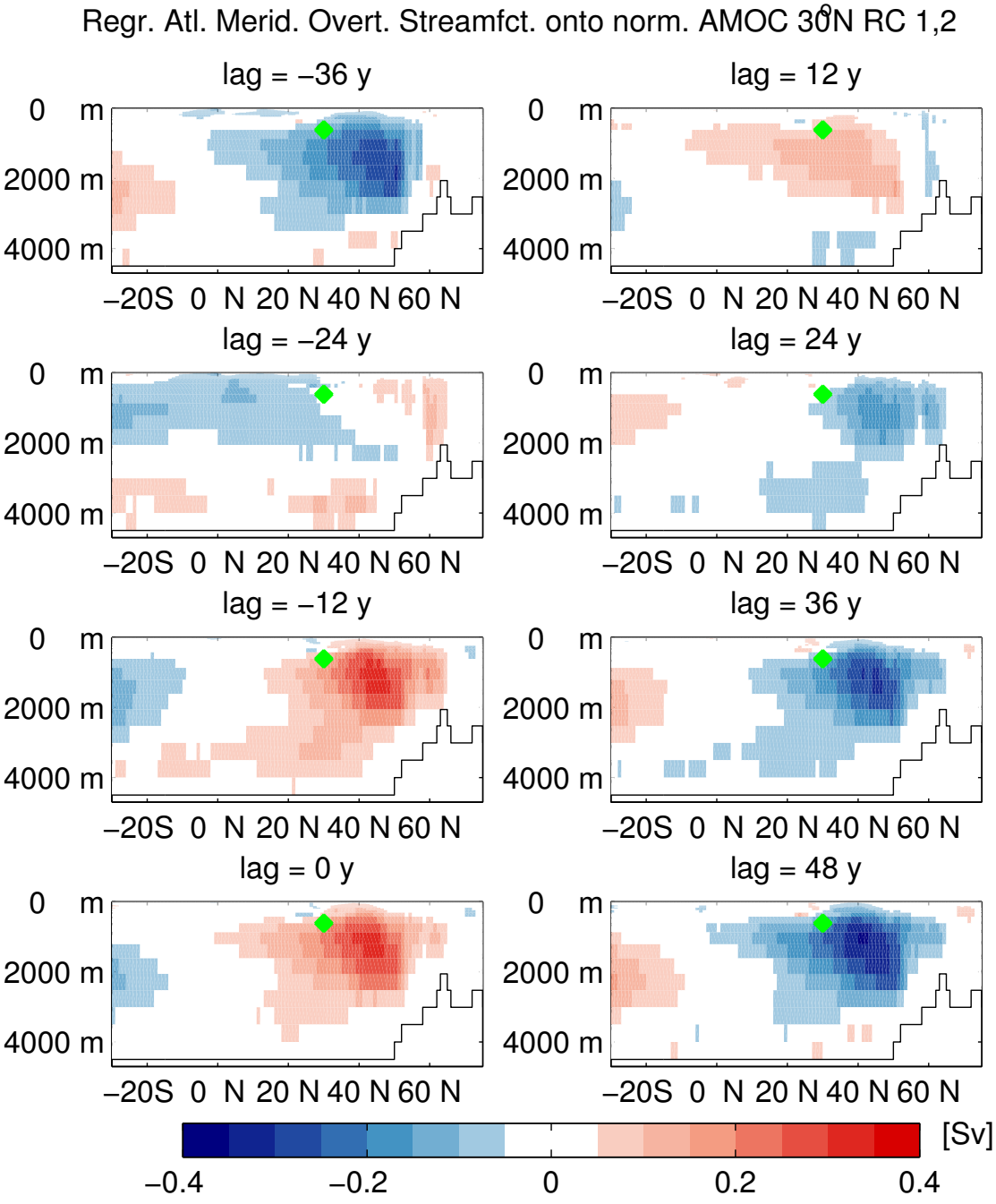

Figure 17: Regression of the Atlantic meridional overturning streamfunction onto the normalized SSA time series reconstructions of the 93 year mode of the AMOC 30°N index for different lags. Positive lags indicate that the index is leading. The green dot indicates where the AMOC 30°N index is located.

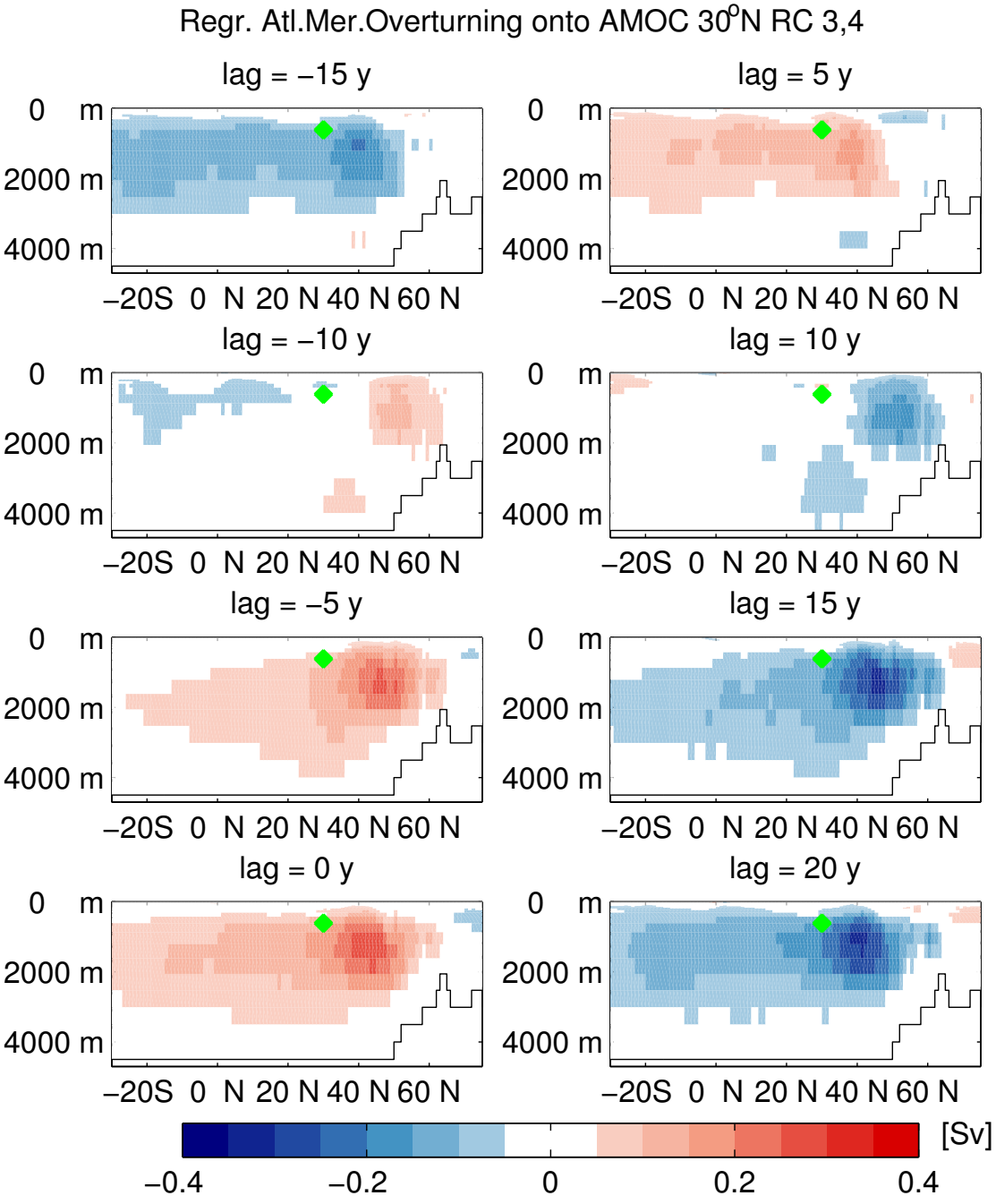

Figure 18: Regression of the Atlantic meridional overturning streamfunction onto the normalized SSA time series reconstructions of the 36 year mode of the AMOC 30°N index for different lags. Positive lags indicate that the index is leading. The green dot indicates where the AMOC 30°N index is located.

Comparing also regression of heat content, the barotropic streamfunction, and the mixed layer depth onto the two AMOC index reconstructions one can see that in both cases the dominant pattern does not change (Figure 19). The variables are leading the AMOC 30°N index by representative time lags, i.e. regressions of other time lags look similar but weaker. These lags match roughly with the first signal evolution in the overturning streamfunction leading the AMOC 30°N index: around 12 years for the longer, and around 5 years for the shorter mode (Figure 17 & 18). These delay times are apparently necessary to transfer the signal from the surface variables (Figure 19) and from the overturning streamfunction center at 45°N (Figure 17 & 18) to the AMOC at 30°N.

The regressions of the heat content (Figure 19 a, b) look very similar to the heat flux forcing pattern (Figure 3b) but with the positive lobe expanding much farther to the northeast. This is probably a result of advection of the warm anomaly with the mean currents. A negative center is located over parts of the subpolar gyre but also the Labrador Sea. The regression onto the longer AMOC mode of 93 years (Figure 19a) is reaching even into the South Atlantic, whereas the regression onto the shorter AMOC mode of 36 years does not. In both cases the meridional gradient in heat content is enhanced before the AMOC at 30°N is following to increase after some years. In the regressions of the barotropic streamfunction (Figure 19 c, d) one can recognize the influence of the NAO forcing (cf. Figure 10b). The anomalies in the tropics and in the southern hemisphere are more related to the longer AMOC mode, whereas, the anomalies around the Gulf Stream region are more influenced by the short mode. The streamfunction in the Labrador Sea is not affected for both modes. The mixed layer depth regression (Figure 19e, f) is again confined to the center of the subpolar gyre region and no response is found in the Labrador Sea. The regression onto the longer AMOC mode is slightly stronger. Therefore, one can conclude that a stronger AMOC is associated with deeper mixed layers in the subpolar gyre region.

CONTROL EXPERIMENT

The variability in the NAO-HF experiments are compared to an unforced KCM control run, (experiment id: W03), of which the boundary forcing is set to present-day values, e.g. CO2=348 ppm. It is 1000 years long but only the last 700 years (years 300 to 999) are used for this analysis. The initial 300 years are skipped as a spin-up stage. The first mode of variability in an EOF analysis with the simulated winter sea level pressure corresponds to the

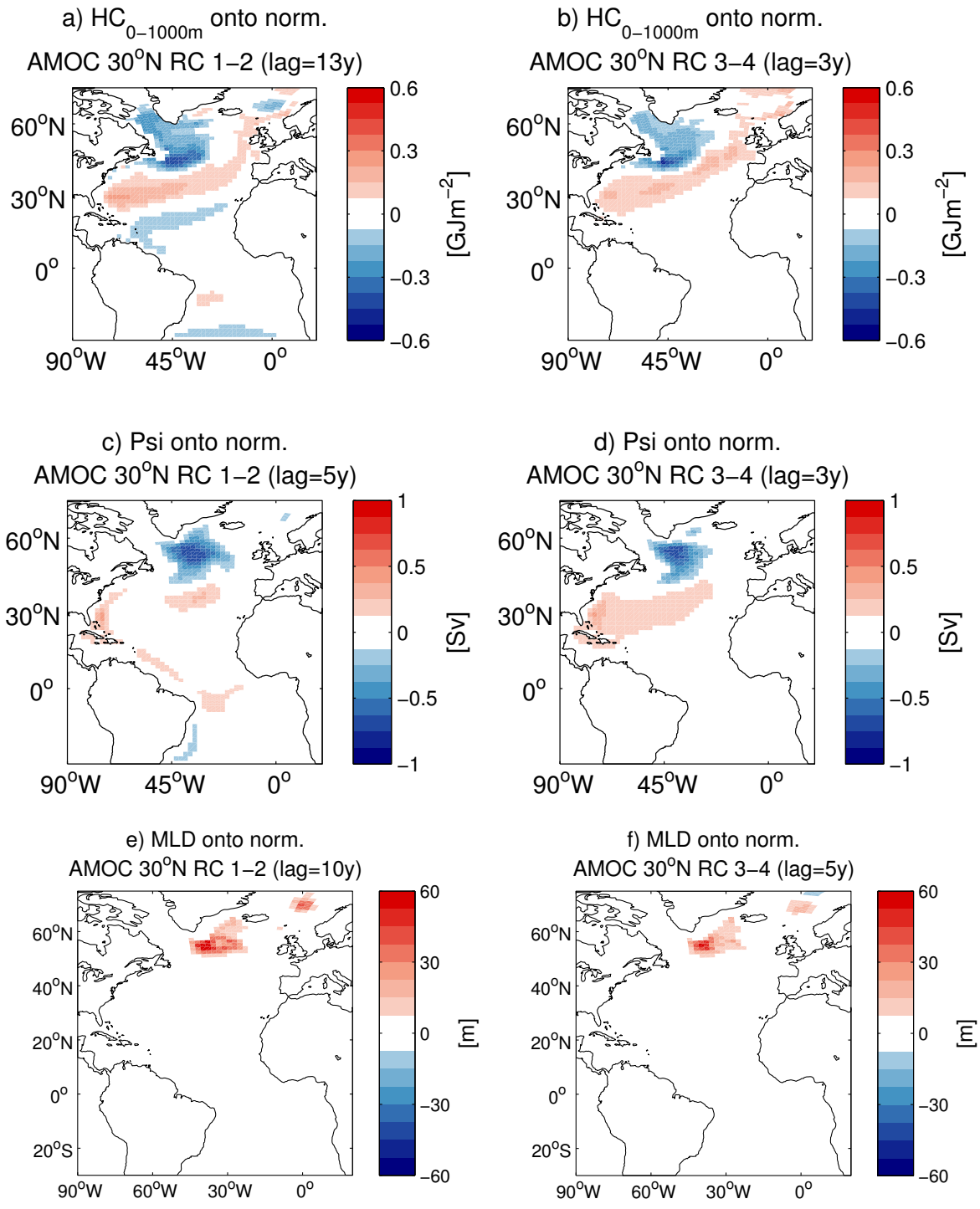

Figure 19: Regression of the upper 1000 m ocean heat content leading by 13 years (a), leading by 3 years (b), of the barotropic streamfunction leading by 5 years (c), leading by 3 years (d), and of the mixed layer depth leading by 10 years (e), leading by 5 years (f) onto the normalized SSA time series reconstructions of the AMOC 30°N index. The AMOC reconstructions are based on the 93 year mode for (a), (c), and (e) and for the 36 year mode in (b), (d), and (f). Positive lags indicate that the variables lead the AMOC 30°N index.

NAO. The pattern consists of a subpolar-to-subtropical dipole (Figure 20a). The associated time series of the NAO index is very similar to the NAO index derived from a station-based calculation (Figure 20b). The correlation coefficient between those two NAO indices is 0.93, which is significant at 95%-confidence. Furthermore, with 46% the NAO mode explains by far the largest amount of variability (Figure 20c). With 1.79 the standard deviation of the station-based NAO index is only slightly smaller than the standard deviation of the station-based Hurrell NAO index from 1900 to 2010, which is about 1.97. In the following analysis, only the station-based version of the NAO index will be used.

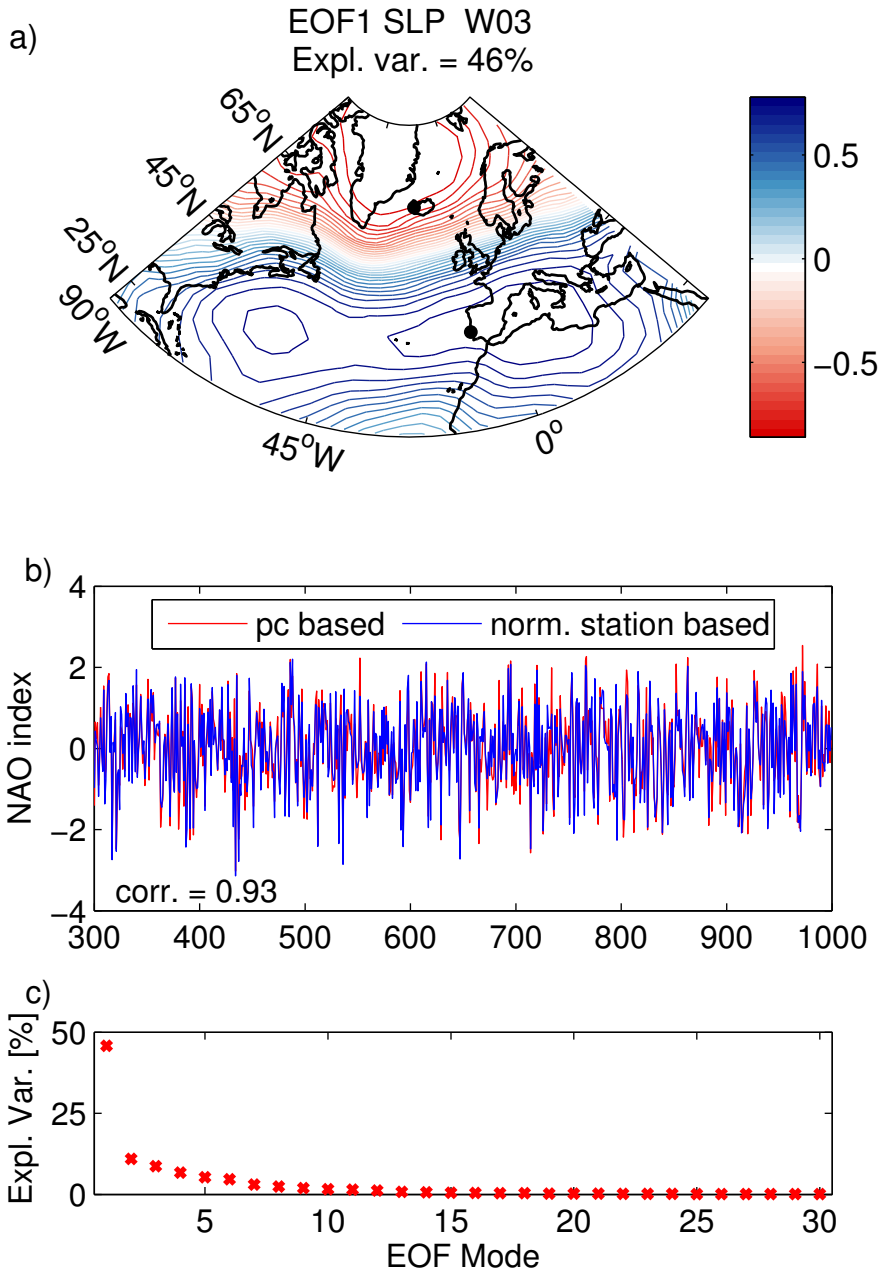

Figure 20: NAO in the W03 control experiment. Shown are a) the EOF based NAO pattern based on winter (December to March) sea level pressure, b) the EOF and normalized station based NAO index, and c) the explained variances of the winter sea level pressure EOF modes.

The relation of the AMOC and the NAO is different from the NAO-HF experiment. The regression pattern of the Atlantic meridional overturning streamfunction onto the NAO index (Figure 21) is strongest when no lag in time is used: A positive NAO index is associated with an increased overturning at 20° to 40°N and a decreased overturning at 50° to 60°N. Both cells are covering nearly the full depth from the surface to the bottom. Just one year later (lag = 1 y) the signs of these cells switch. Now, the location of the AMOC 30°N index is even closer to the center of the variability cells. Regressions for longer time lags are weak compared to the ones shown in Figure 21. The relation of both variables is only present on very short time scales compared to the NAO-HF conditions.

The spectrum of the NAO index (Figure 22) is close to a white noise spectrum but with significant peaks mainly on interannual time scales and the largest one at a period of about 10 years. The spectrum of the AMOC (Figure 23) behaves similar to red noise but with significant variability at centennial to multi-centennial but also at interannual time scales.

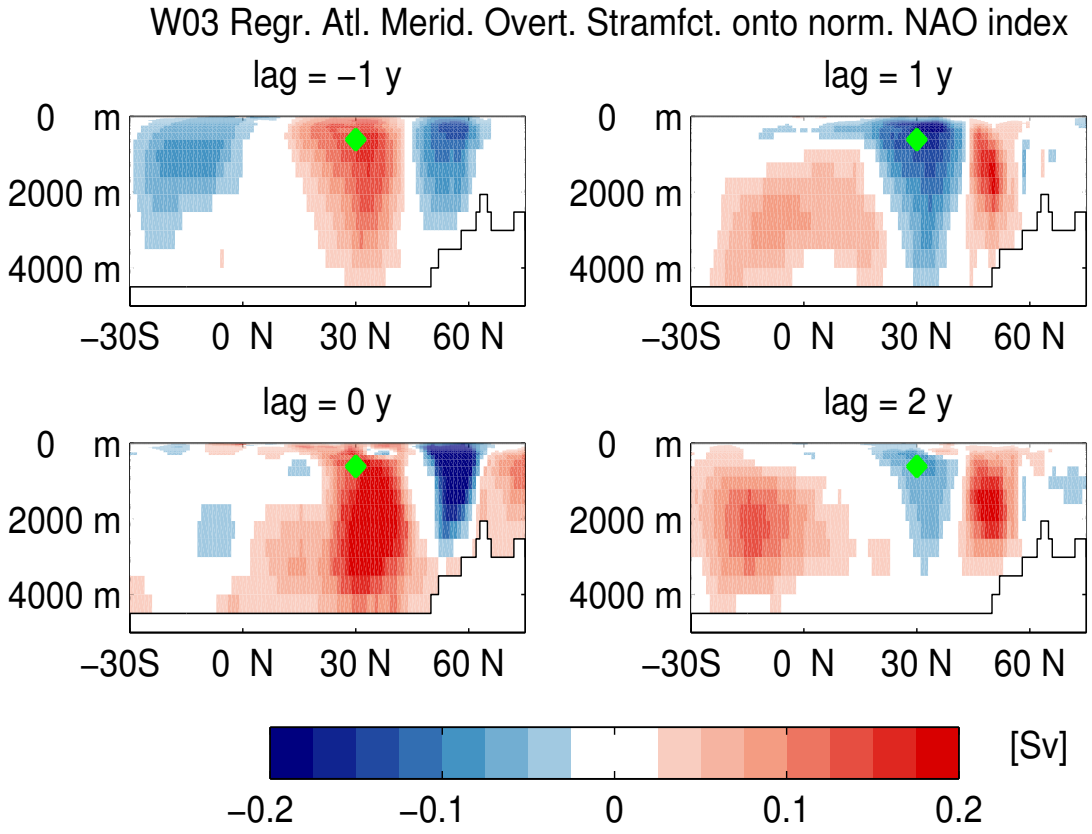

Figure 21: Regression of the Atlantic meridional overturning streamfunction onto the normalized NAO index in the control experiment for different lags. Positive lags indicate that the index is leading. The green dot indicates where the AMOC 30°N index is located.

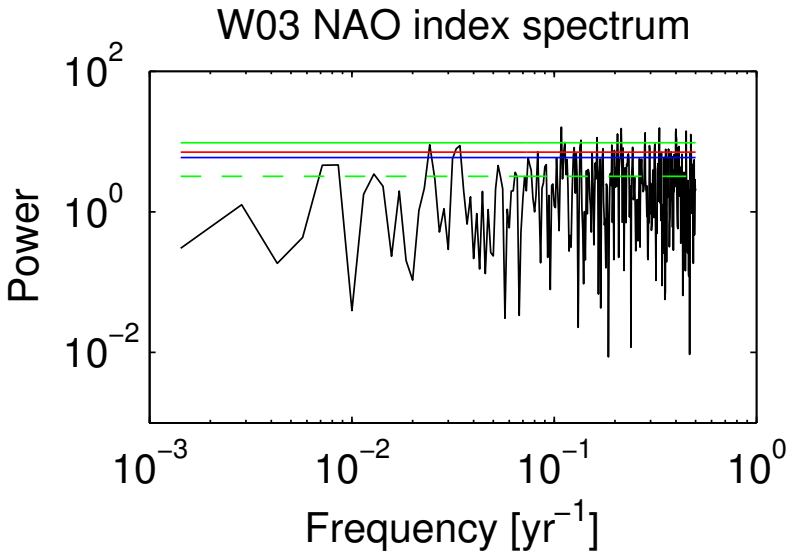

Figure 22: Power spectrum of the NAO index in the control experiment. The green dashed line indicates the spectrum of a white noise process, the blue line its 90%-, the red line its 95%-, and the green solid line its 99%-confidence limit.

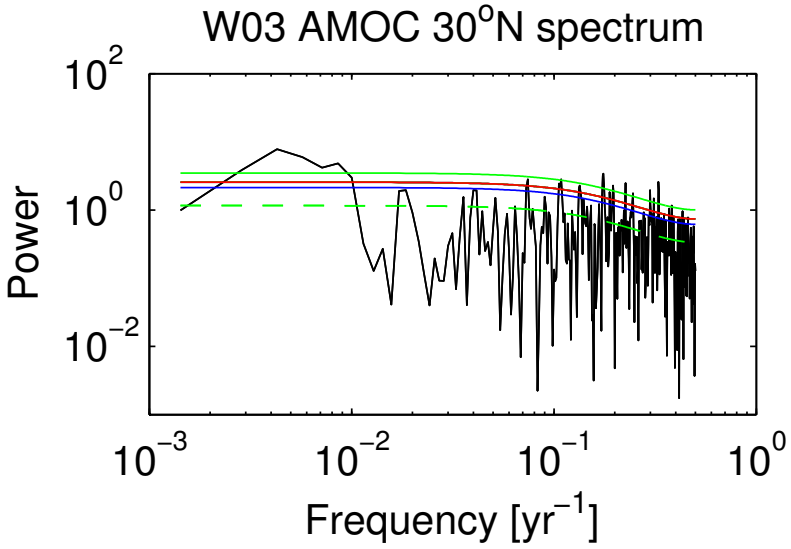

Figure 23: Power spectrum of the AMOC 30°N index in the control experiment. The green dashed line indicates the spectrum of an autoregressive process, the blue line its 90%-, the red line its 95%-, and the green solid line its 99%-confidence limit.

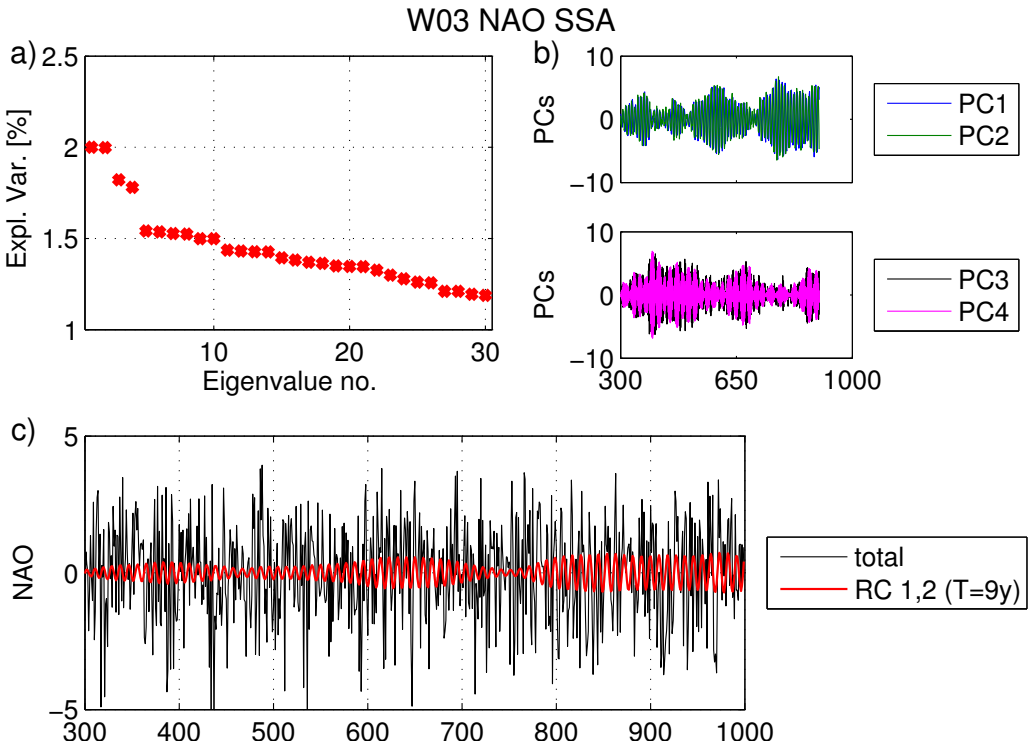

Figure 24: SSA results of the control experiment for the NAO index with a window length of 56 years. Shown are the percentages of explained variance (a), and for the leading modes also the principal-components (b) and the time series reconstruction (c).

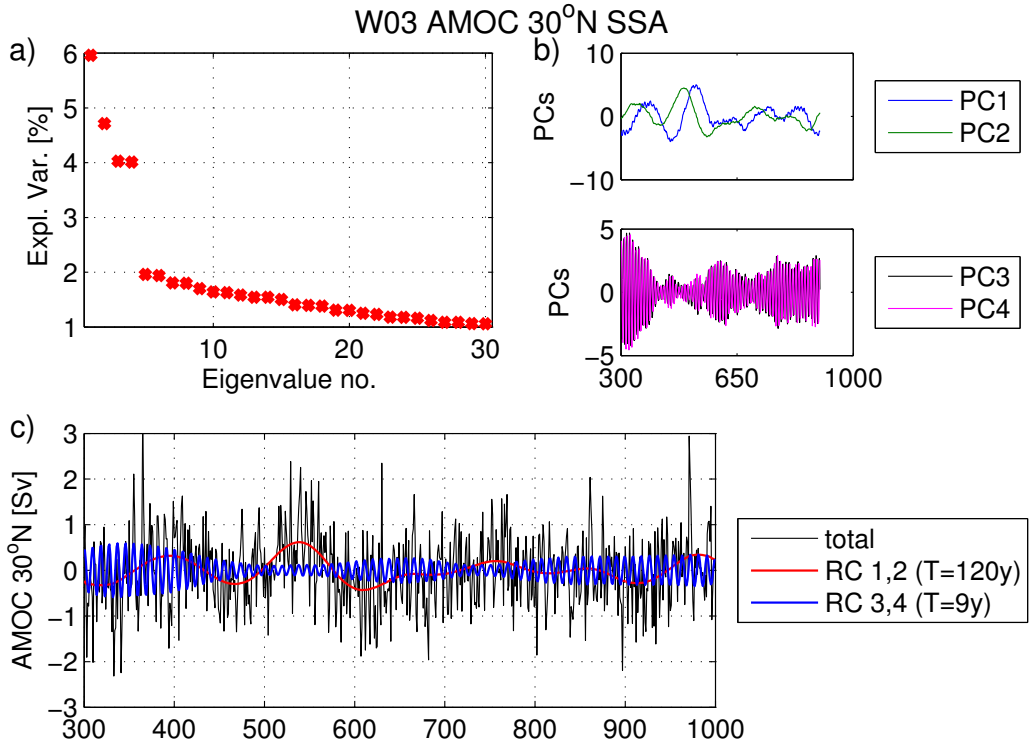

Figure 25: SSA results of the control experiment for the AMOC 30°N index with a window length of 56 years. Shown are the percentages of explained variance (a), and for the leading modes also the principal-components (b) and the time series reconstruction (c).

Following SSA with a window length of 100 years, the NAO index has a dominant mode at a period of 9 years (Figure 24). This period is also found for the AMOC 30°N index, where it explains about 9% of the total variance (Figure 25). This mode is significant against red noise at a confidence level of 95% for both variables (see Figure A18 & A19 in the appendix). A variability mode of about 120 years is explaining even 11%, but its oscillation is not so stable in amplitude and in period.

The different dynamical relation between the AMOC and the NAO and the importance of the 9 year mode is also evident in the time series. The NAO index is represented by its dominant 9 year mode (Figure 26) but the full AMOC 30°N variability is shown. For some periods it looks like the AMOC 30°N index is leading the NAO index reconstruction by 1 year. This is also supported by the cross-correlation (Figure 27) which has a significant peak of 0.2 for this lag. Compared to that, the correlation in the case of no lag is smaller here, but this is due to the location of the AMOC 30°N (green dot in Figure 21) relative to the center of variability.

The interannual to decadal variability is apparently more pronounced in the control compared to the forced experiment. The slow 120 year mode, however, found in the SSA of the AMOC 30°N index is not stable. Wavelet analysis of the AMOC index (Figure 28) reveals that this variability mode is only present in the simulation from the year 300 to 650 approximately. Significant power is only found for periods of about 10 years and lower. In addition, the wavelet result supports that neglecting the first 300 years as a spin-up phase was the right choice, because its spectrum is inconsistent with the following 700 years.

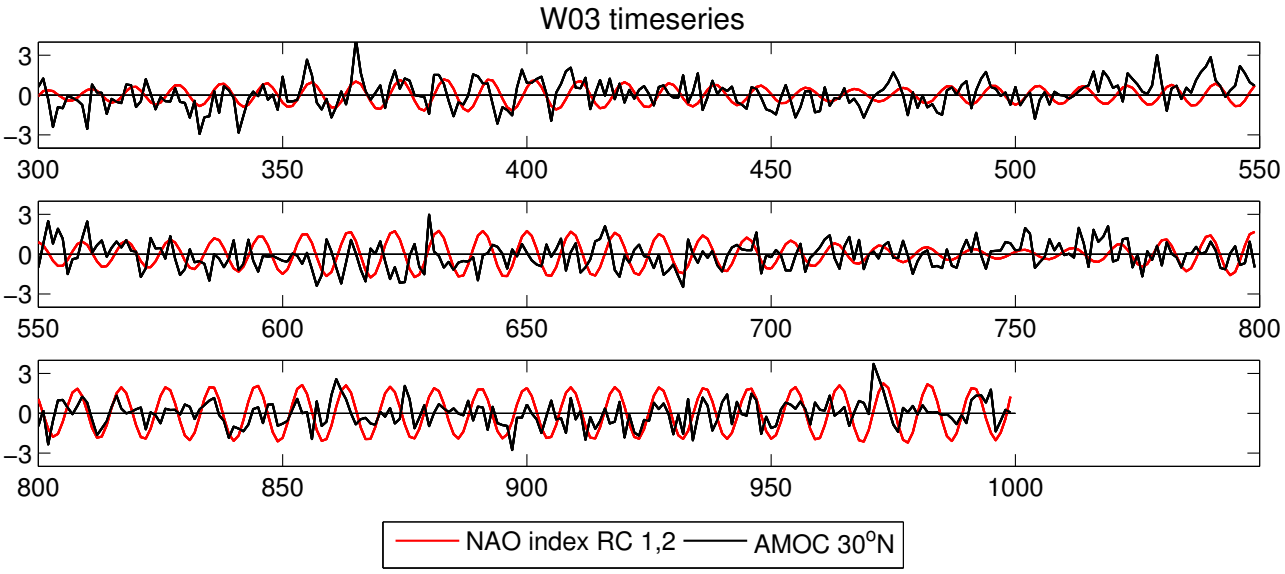

Figure 26: Time series of the AMOC 30°N index and the SSA NAO reconstruction based on its 9 year mode in the control experiment.

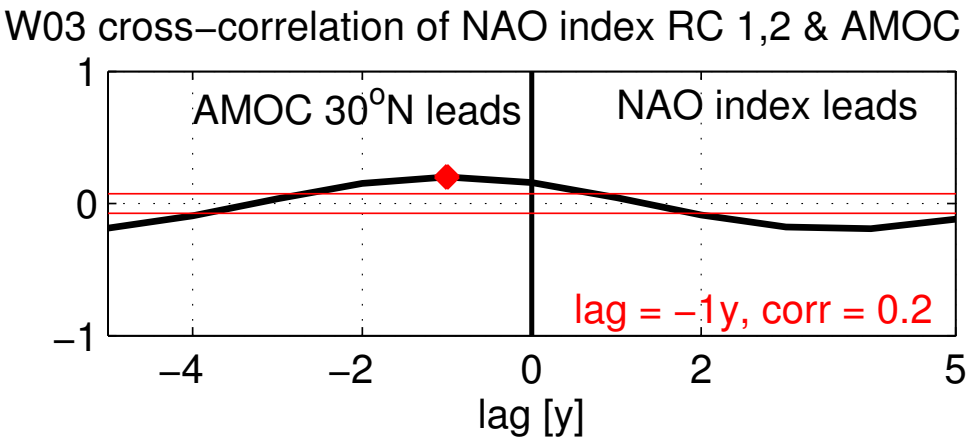

Figure 27: Cross-correlation between the AMOC 30°N index and the SSA NAO reconstruction based on its 9 year mode in the control experiment. The red horizontal lines indicate the 95%-confidence intervals.

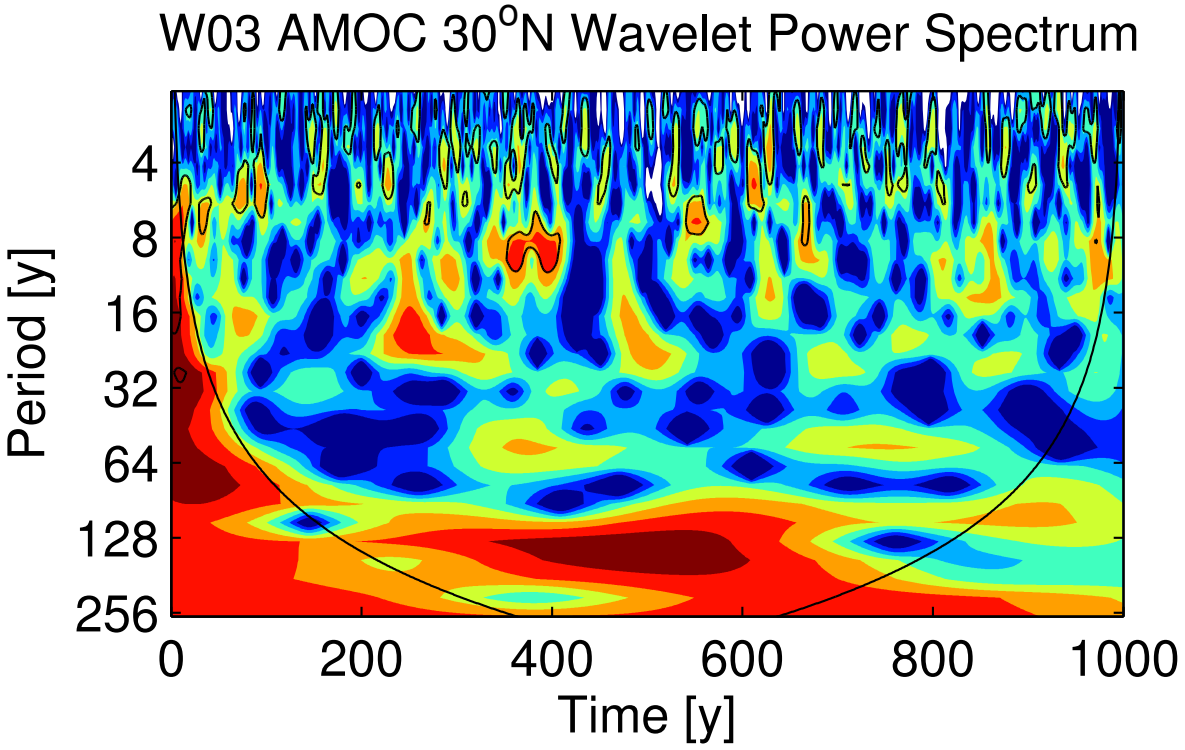

Figure 28: Wavelet power spectrum of the AMOC 30°N index in the control experiment. The contoured areas indicate significance against red noise based on a 95%-confidence level.

IV) SUMMARY & DISCUSSION

The AMOC variability of the KCM was investigated under heat flux forcing anomalies associated with the NAO. This experiment was labeled NAO-HF.

The heat flux tripole pattern (Figure 3b) is the short-term response caused by the NAO which reflects also in SST (Visbeck et al., 2003; Eden & Willebrand, 2001; Álvarez-García et al., 2008). Even in neutral NAO winters there is a large heat loss in the west of the subpolar North Atlantic to the atmosphere. In a positive NAO phase the increased westerlies enhance the energy loss of the ocean in this region leading to stronger deep-convection. Observations support the connection of NAO forcing and an increased Labrador Sea convection (Pickart et al., 2002).

The AMOC represented by the meridional overturning streamfunction (Figure 5a) seems to be well simulated with a stronger positive cell at the top and a weaker negative cell at the bottom. The upper cell is sometimes called North Atlantic Deep water (NADW) cell, because it transports NADW generated in the subpolar North Atlantic towards the Southern Ocean. The bottom cell, in contrast, transports Antarctic Bottom Water (AABW) from the Southern Ocean into the North Atlantic. The long-term mean of the maximum overturning of about 16 Sv is close to the 19 Sv observed at 26.5°N (Cunningham et al., 2007). However, in the KCM simulations a known temperature bias at the surface exists in the North Atlantic: The northward component of the Gulf Stream path is too weak. This causes the North Atlantic to be too cool over large parts (see also Figure A1, appendix). This bias has been discussed also in other model studies (Smith et al., 2000) and methods to overcome this problem were suggested, for example, by Eden et al. (2004). In the mean state of mixed layer depth the Labrador Sea and consequently the convection in this region is underestimated (Figure 5c). Instead, the area of the subpolar gyre (box in Figure 5d) has by far the largest mixed layer depth. This error might also be related to the cold SST bias and associated with that the coverage with sea ice, but it must also have further reasons. Some studies suggest that the role of the Labrador Sea is dominant within the North Atlantic deep-convection (e.g., Eden & Willebrand, 2001), but different studies state that other convection sites are more important (e.g., Pickart & Spall, 2007).

The 11-year running mean time series (Figure 6) reveal that there is pronounced multi-decadal variability also in the reanalysis NAO index. This suggests that there is some influence from ocean-atmosphere coupling. One can see that the mixed layer depth responds immediately to

the NAO forcing, and that the subpolar gyre strength just after 1 to 2 years. It takes somewhat longer, about 3 to 14 years, until the signal of increased deep water formation is reflected in the increased AMOC at 30°N (cf. also Figure 7c). This is not surprising, taking into account that this index is defined at a depth of about 600m and that adjustments of the deeper ocean are slow compared to the surface. Furthermore, the index of 30°N is placed much more in the south than the convection region from which the signal might arise. Indices of the AMOC of more northward latitudes are therefore responding earlier (Figure A2, appendix). Thus, except of the years before 1934, which could still be influences by some spin-up effects, the AMOC index and the other variables behave similar and seem to follow the NAO index quite well.

This is supported by the lagged regression patterns of the overturning onto the NAO index (Figure 9). A positive NAO index causes an enhanced convection and a stronger overturning. In the direct regression without a lag in time no signal is present at the location of the AMOC 30°N index (green dot). The dominant response is a positive signal with a center around 45°N in a depth of about 500 to 2000 m. This immediate response pattern might also be influenced by momentum flux anomalies and corresponding Ekman transport and Ekman convergence. This process is suggested to play an important role for the immediate response of the ocean to NAO forcing (Visbeck et al., 2003). However, in this experiment the simulated wind anomalies due to the NAO will probably look different than in the observations, but this is not analyzed in further detail here. After 5 years the positive signal has expanded mainly downwards and southward. At even longer lags the signal becomes shallower again and propagates further into the south.

Like in the mean state of the mixed layer depth, its regression onto the NAO (Figure 10a) reveals that the Labrador Sea is not sensitive to NAO forcing. This differs from the results of Eden & Willebrand (2001) who showed the ocean response to NAO hat flux forcing is restricted to the forcing located in the Labrador Sea. This disagreement is a result of the KCM bias in the North Atlantic. On the other hand, there is agreement with the results of Eden & Willebrand (2001) with regard to the stronger subpolar gyre (negative anomaly of a negative mean state) due to increased ocean heat loss (Figure 10b) which is present in a positive NAO phase.

The modes of variability were analyzed via Singular Spectrum Analysis (SSA). Comparing the resulting explained variance of the eigenvalues reveals that only in the case of the AMOC but not for the NAO index there is a clear separation of the first dominant modes compared to the noisy rest (Figure 12a and 13a). Two oscillatory pairs consisting of the first 4 eigenvalues

are explaining 51 % of the entire variance of the AMOC. In contrast, the NAO exhibits a variability that is only slightly red. Nevertheless, a red spectrum would be unusual for a purely atmospheric variable. The NAO index, however, might also be influenced by anomalies of the ocean (Czaja et al., 2003) which could enhance lower frequencies in the NAO like the 58 year mode.

The period of 8 years in the pair of eigenvalues 3 and 4 matches the 8 to 10 year peak of the observed NAO spectrum (Hurrell et al., 2003). Furthermore, it is also the period of the dominant mixed layer depth mode (Figure 16a). It responds nearly rapidly to the NAO forcing. The 58 year mode of the NAO index is more pronounced in the second half of the 20^{th} century. It describes also the positive trend in the NAO index from the 1960s to the 1990s. This trend was often discussed as a signal of anthropogenic climate change (Gillet et al., 2003). However, the recent retreat to low NAO indices after the year 2000 and a much weaker trend projected by models suggest an internal cause (Osborn, 2011).

Among the AMOC modes, most variance is explained by a mode of about 93 years period, and second most by a 36 years period (Figure 13c). A quasi-centennial mode of about 100 years period and a multi-decadal mode of about 60 years period were found in the P86 control experiment of the KCM (Park & Latif, 2012). The 93 year mode found here might be connected to their quasi-centennial mode. Though, Park & Latif (2012) related the quasi-centennial mode to salinity advections from lower to higher latitudes. The NAO-HF experiment, however, is driven only by heat flux forcing. It is possible that this forcing influences also the salinity advection, e.g. through the anomalies in the subtropical and subpolar gyre. This was not analyzed here, but could be an important process for the interaction of the gyre circulation and the AMOC. They furthermore related the multi-decadal mode to surface flux anomalies originating in the subpolar regions of the North Atlantic. This mode has also been associated with NAO forcing (Delworth & Greatbatch, 2000). In a study of Zhu and Jungclaus (2008) two AMOC modes were found in the ECHAM5/MPIOM coupled model: a 60 year mode that is only present when ocean and atmosphere are fully coupled, and a 30 year mode which is present without an interacting atmosphere.

The first mode of subpolar gyre strength is of about 80 years period and the mixed layer depth index includes a component of roughly 84 years. The similar behavior of these components and the long AMOC mode could be caused by a long-term response of the ocean involving a feedback connecting these variables, for example, as suggested by Ba et al. (2013).

Lagged regressions of the whole overturning streamfunction onto the reconstructed AMOC 30°N index (Figure 17 and 18) show that the reaction of both modes is very similar regarding the spatial structure. In both cases the center of the signal is placed more northward and deeper than the AMOC 30°N index. Still, a difference can be found: The pattern of the 93 year mode seems to be more vertical and not so uniformly expanded in the horizontal.

In the regression of upper ocean heat content and the barotropic streamfunction onto the two AMOC modes one can see that the longer 93 year mode (Figure 19a,c) is not entirely confined to the northern hemisphere as in the case of the 36 year mode (Figure 19b,d). Nevertheless, the regressions in the southern hemisphere of the 93 year mode are weak compared to the North Atlantic, which is reasonable with a forcing located only over the northern hemisphere. At least for multi-centennial modes, the southern hemisphere and especially the Southern Ocean is suggested to play an important role (Latif et al., 2013; Martin et al., 2013). Unfortunately, the length of this experiment makes it impossible to analyze such time scales. Furthermore, the signal in the Labrador Sea heat content is not surprising as the negative heat flux signal of a positive NAO forcing is spreading over the whole subpolar gyre and also the Labrador Sea (Figure 3b). Nevertheless, there is no convection signal in the Labrador Sea (Figure 10a) due to the KCM SST bias with sea ice cover and maybe further errors in this region.

Finally it should be noted, that this experiment did not include momentum, and freshwater forcing associated with the NAO. In another experiment the KCM was forced by global wind ERA-40 (Uppala et al., 2005) and NCEP/NCAR reanalysis data. It was run only for a period of 44 years and it seemed to be strongly influenced by model spin-up. The results are not shown, but it should be mentioned that the AMOC variability of this experiment is larger and mainly interannual. In addition, it was tested if certain modes of the NAO-HF and the wind experiment coincide, but no consistency was found.

This NAO heat flux experiment involved prescribed heat flux forcing. Nevertheless, the atmosphere could also be influenced by the ocean response through feedback mechanisms (Kushnir et al., 2002; Czaja et al., 2003). Only responses of the ocean to the atmosphere were analyzed in this thesis, but for further analyses the reversed direction of ocean-atmosphere interaction might also be of interest.

The spatial NAO pattern in the KCM control simulation is quite similar to the NAO obtained from reanalysis data (see Figure A17, appendix). Still, the low pressure center is shifted

slightly to the Northwest. Large differences between the control and the NAO-HF experiment are found for the dynamical relation of the AMOC and the NAO. The spectrum of the NAO index is closer to a white noise spectrum (Figure 22) than the NAO index in the NAO-HF experiment (Figure 11).

The regression pattern of the AMOC onto the NAO index (Figure 21) is very different from the NAO-HF simulation and it acts furthermore on a shorter time scale. The pattern is stretched more in the vertical and less in the horizontal compared to the NAO-HF experiment (Figure 9). In the latter, the center of the signal was located at around 45°N. In the control experiment, however, 45°N is the border between the positive and the negative cell. Furthermore, the control pattern switches very fast within one year. But in the NAO-HF experiment the response of the AMOC was slow and it took 3 to 14 years for it to develop. Also the dominant modes show a very different behavior (cf. Figure 17 & 18 vs. Figures A20 & A21 in the appendix). One can conclude that in the control simulation further processes are important for the relation of the AMOC and the NAO. In the NAO-HF experiment the heat flux was prescribed and a feedback of the ocean back to the NAO was not possible. Besides such a feedback mechanism, the AMOC response to NAO wind anomalies and corresponding Ekman transport anomalies might also be important in the control simulation. Also the comparison of variability modes emphasizes the faster interaction between AMOC and NAO in the control simulation. For both variables there is a 9 year mode (Figure 24 and 25). One slower mode of roughly 120 years was found for the AMOC 30°N index, but it is not very stable (Figure 28). It is strong before the year 650, but after that it becomes very weak and only the periods of less than 10 years stay dominant.

The AMOC 30°N variability of the control experiment is compared with another control run of the KCM as described in Park & Latif (2008, 2010, 2012). That simulation used different parameters, e.g. in the sea ice model. They found three modes of variability in the AMOC, a multi-decadal, a quasi-centennial, and a multi-centennial. In the present simulation, W03, the multi-decadal component of about 60 year periodicity is hardly detectable such that it is lower than the 95%-confidence level (Fig. 23) but multi-centennial variability is significant. Nevertheless, the strongest mode found in this simulation is on decadal time scales as indicated by the first SSA mode (Figure 25c). These differences can be explained by the fact that the KCM control integration used by Park & Latif (2012) is with 4200 years long enough to detect longer variability modes with statistical significance. They used also a larger window length of 300 years and smoothed the data by a 11-year running mean. On the other

hand, they skipped a longer spin-up phase (more than 800 years). Thus, regime changes in the variability spectrum could have happened in the coupled model presented here. Such a regime shift of AMOC variability was also discussed by Kwon & Frankignoul (2012). They suggest that this shift in their results might be caused by a change in the strength and pattern of the subpolar gyre.

Finally, one can conclude that the low frequency component of the heat flux forcing has an obvious effect on the AMOC and that the dominant variability modes of the AMOC have changed compared to the unforced control simulation. Not clear remains which dynamical differences exist between the two AMOC modes of 93 and 36 years. The advection of salinity within anomalous currents might be of further interest even in an experiment with heat flux forcing.

APPENDIX

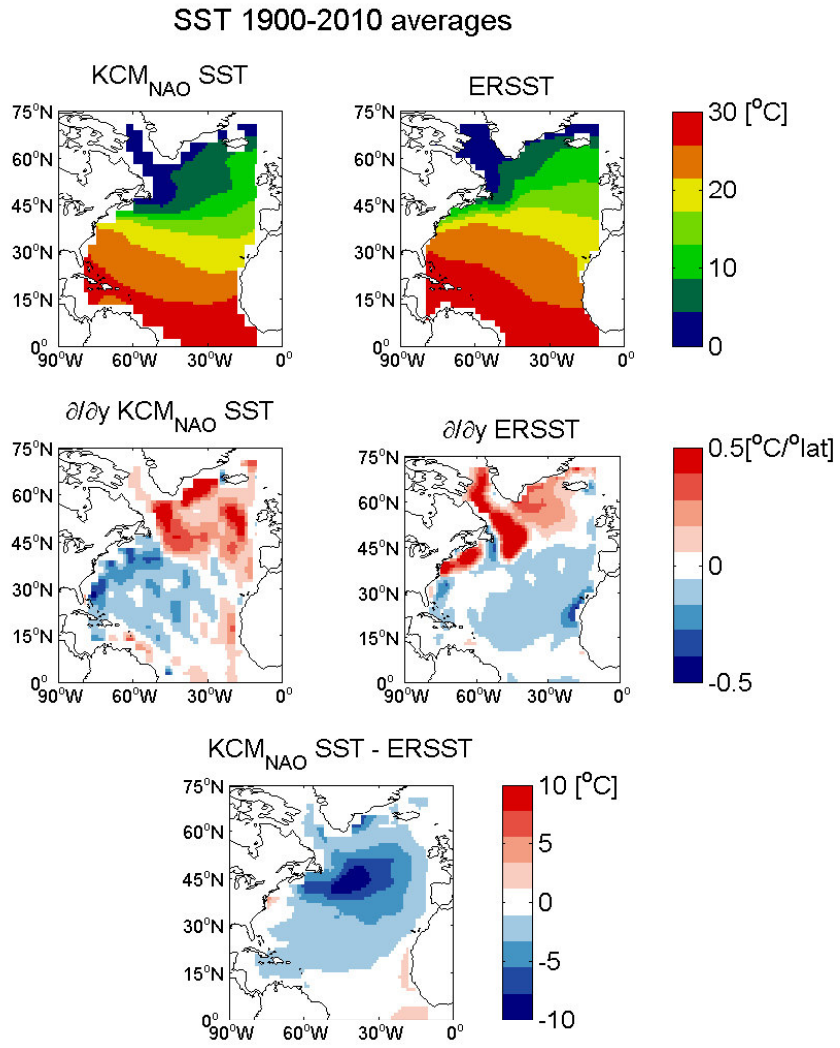

Figure A1: Comparison of sea surface temperature (SST) between the NAO heat flux experiment and ERSST (reconstructed observation)

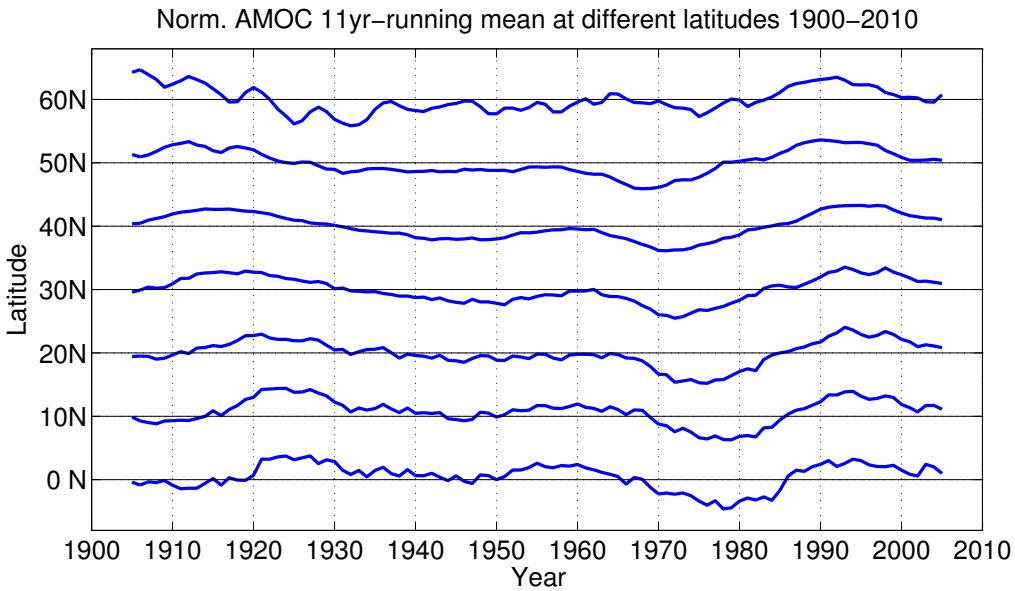

Figure A2: Normalized 11yr-running mean AMOC index of different latitudes

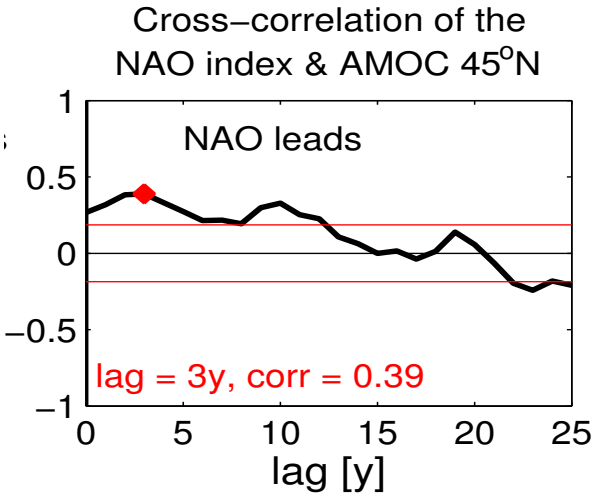

Figure A3: Cross-correlation between the NAO index and the AMOC 45°N index. The red horizontal lines indicate the 95%-confidence intervals.

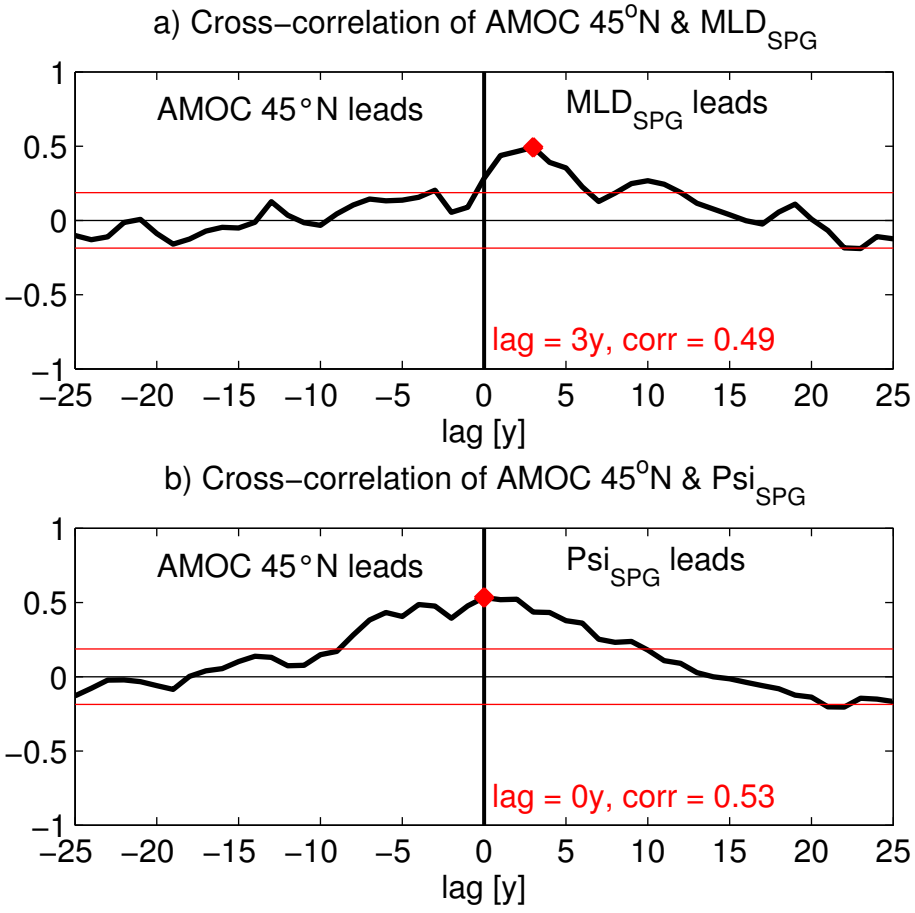

Figure A4: Cross-correlation between the AMOC 45°N index and the mixed layer depth of the subpolar gyre (a) and the AMOC 30°N index and the subpolar gyre strength (b). The red horizontal lines indicate the 95%-confidence intervals.

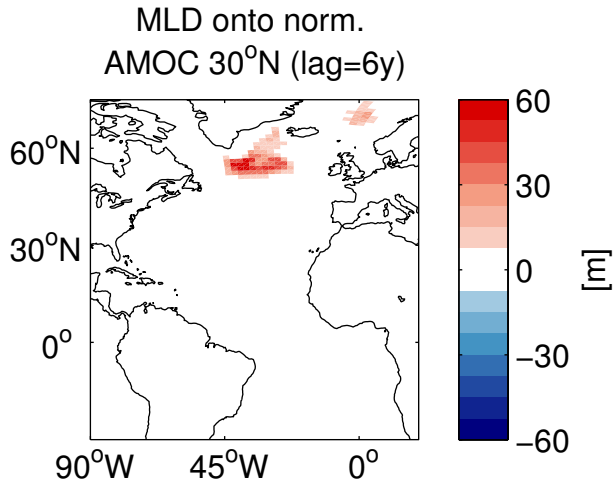

Figure A5: Regression mixed layer depth onto the normalized AMOC 30°N index with the mixed layer depth leading by 6 years. For other lags in time the pattern does not differ and might only be weaker.

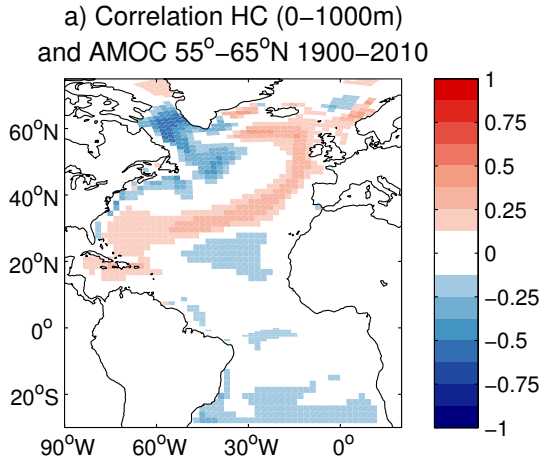

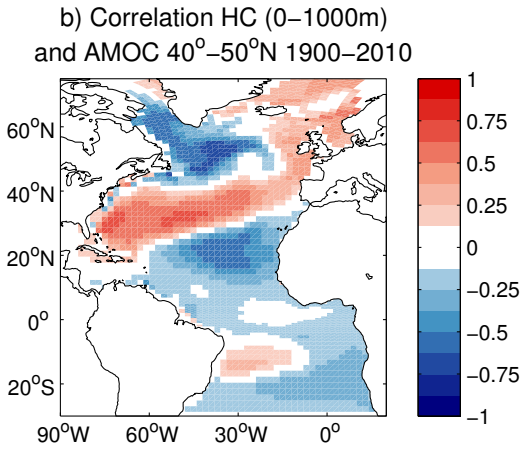

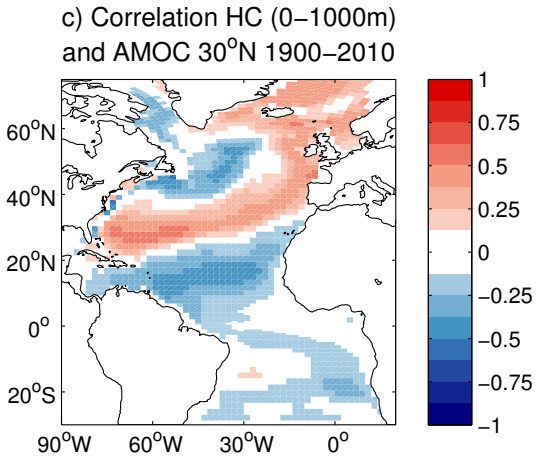

Figure A6: Correlations of ocean heat content of the upper 1000 m and the AMOC index at a) 55°-65°N, b) 40°-50°N, c) 30°N

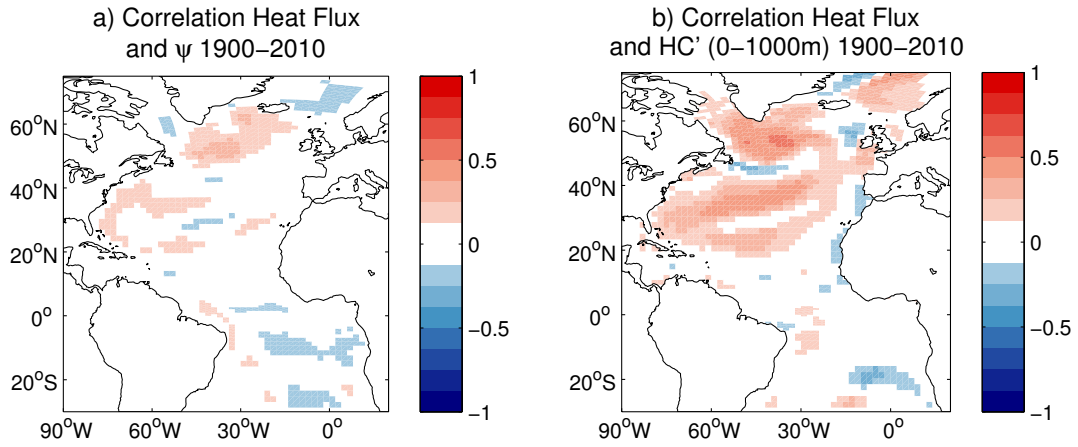

Figure A7: Correlation of heat flux and at a) barotropic streamfunction, b) time derivative of ocean heat content of the upper 1000 m

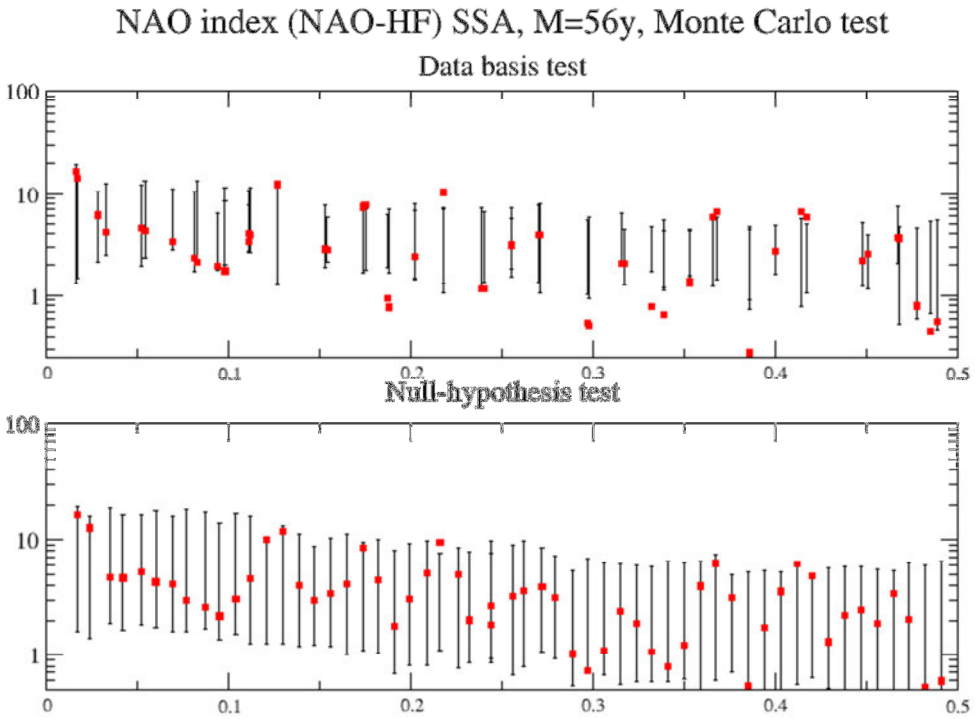

Figure A8: Power of the different SSA frequency modes of the NAO index in the NAO-HF experiment. The bars indicate the 95%-confidence interval of a red noise process derived from 100 Monte Carlo realizations. In the upper panel a data-adaptive and in the lower panel a null hypothesis-based test was carried out.

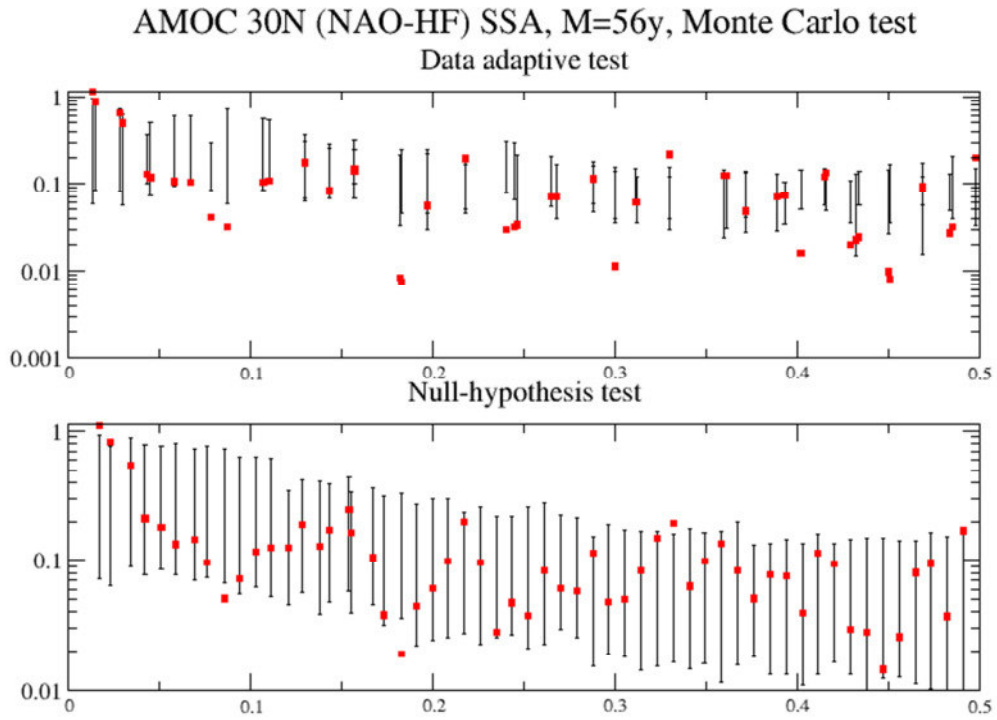

Figure A9: Power of the different SSA frequency modes of the AMOC at 30°N in the NAO-HF experiment. The bars indicate the 95%-confidence interval of a red noise process derived from 100 Monte Carlo realizations. In the upper panel a data-adaptive and in the lower panel a null hypothesis-based test was carried out.

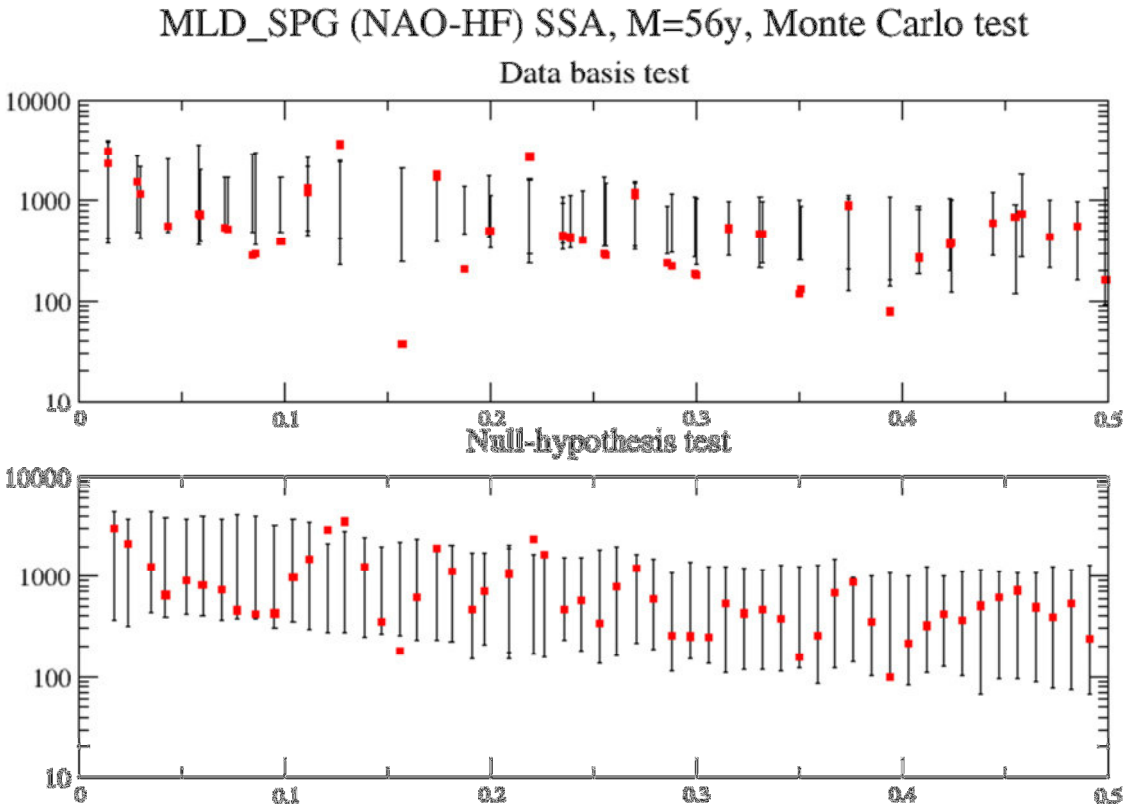

Figure A10: Power of the different SSA frequency modes of the mixed layer depth averaged of the subpolar gyre in the NAO-HF experiment. The bars indicate the 95%-confidence interval of a red noise process derived from 100 Monte Carlo realizations. In the upper panel a data-adaptive and in the lower panel a null hypothesis-based test was carried out.

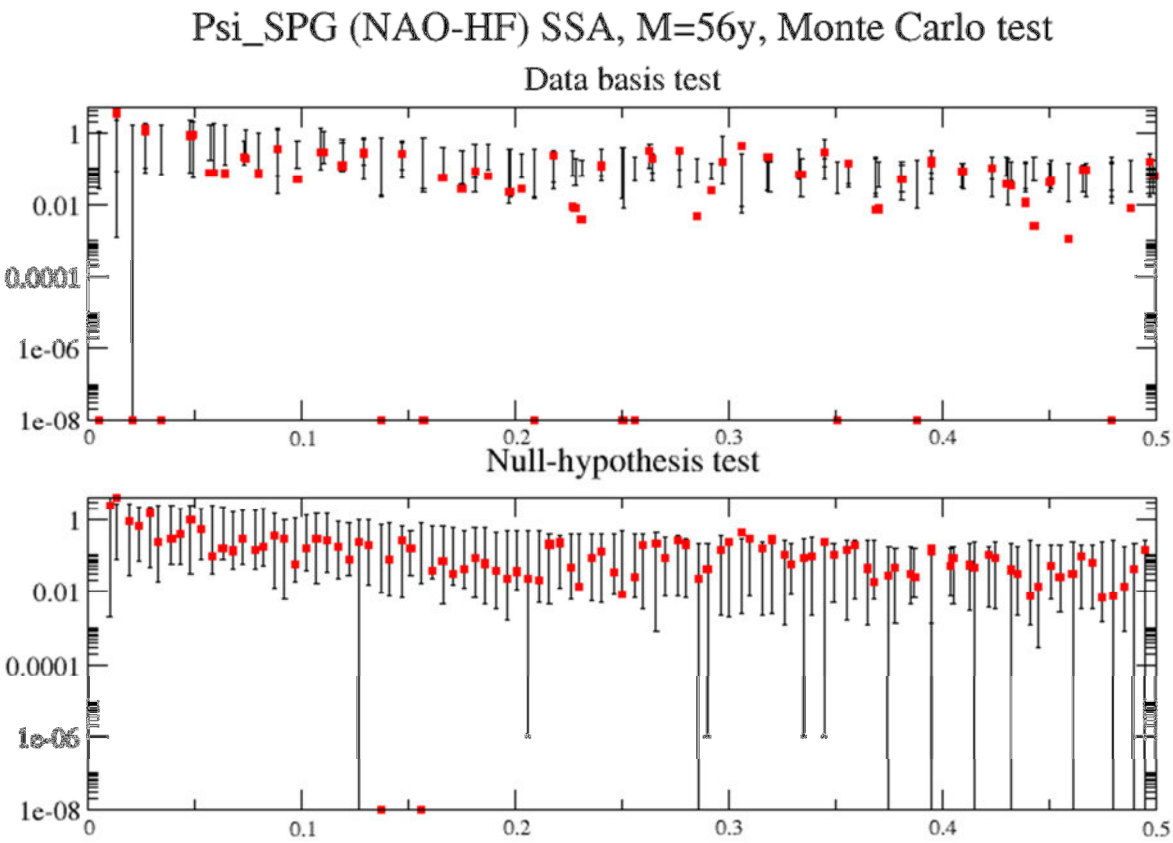

Figure A11: Power of the different SSA frequency modes of the subpolar gyre strength in the NAO-HF experiment. The bars indicate the 95%-confidence interval of a red noise process derived from 100 Monte Carlo realizations. In the upper panel a data-adaptive and in the lower panel a null hypothesis-based test was carried out.

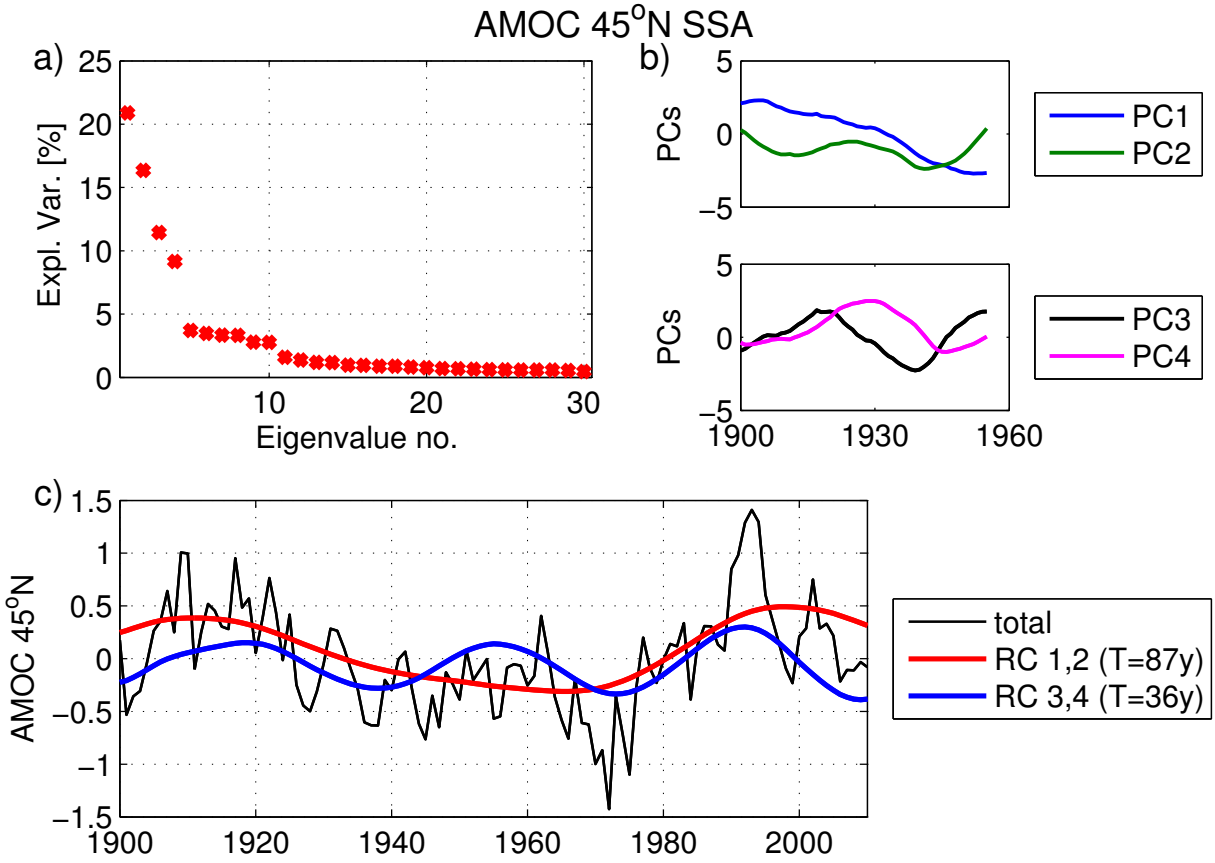

Figure A12: SSA results for the AMOC 45°N index with a window length of 56 years. Shown are the percentages of explained variance (a), and for the leading modes also the principal-components (b) and the time series reconstruction (c).

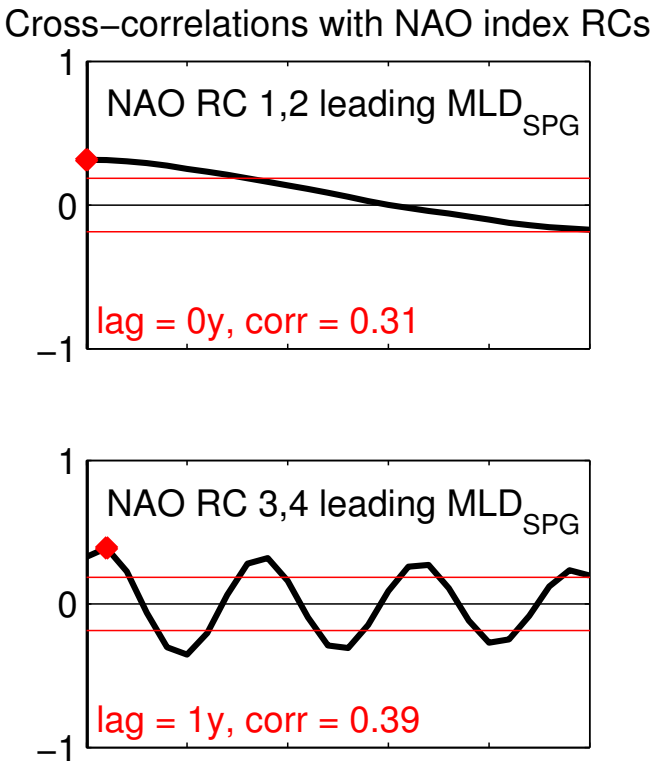

Figure A13: Cross-correlation between the mixed layer depth averaged over the subpolar gyre and a) the 56 year mode of the NAO index, b) the 8 year mode of the NAO index. The red horizontal lines indicate the 95%-confidence intervals.

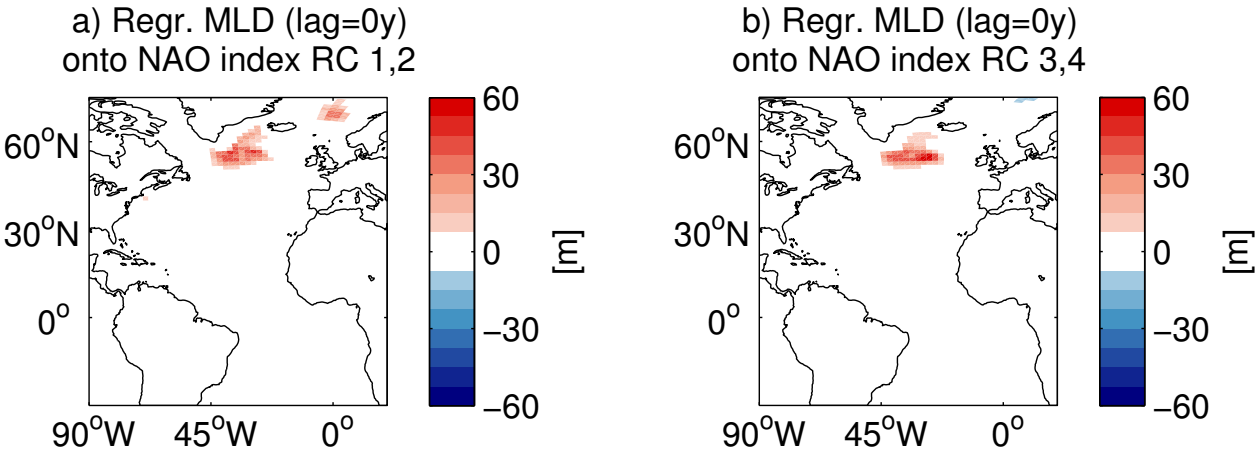

Figure A14: Regression of the mixed layer depth onto the normalized reconstruction of the a) 56 year mode of the NAO index, b) 8 year mode of the NAO index.

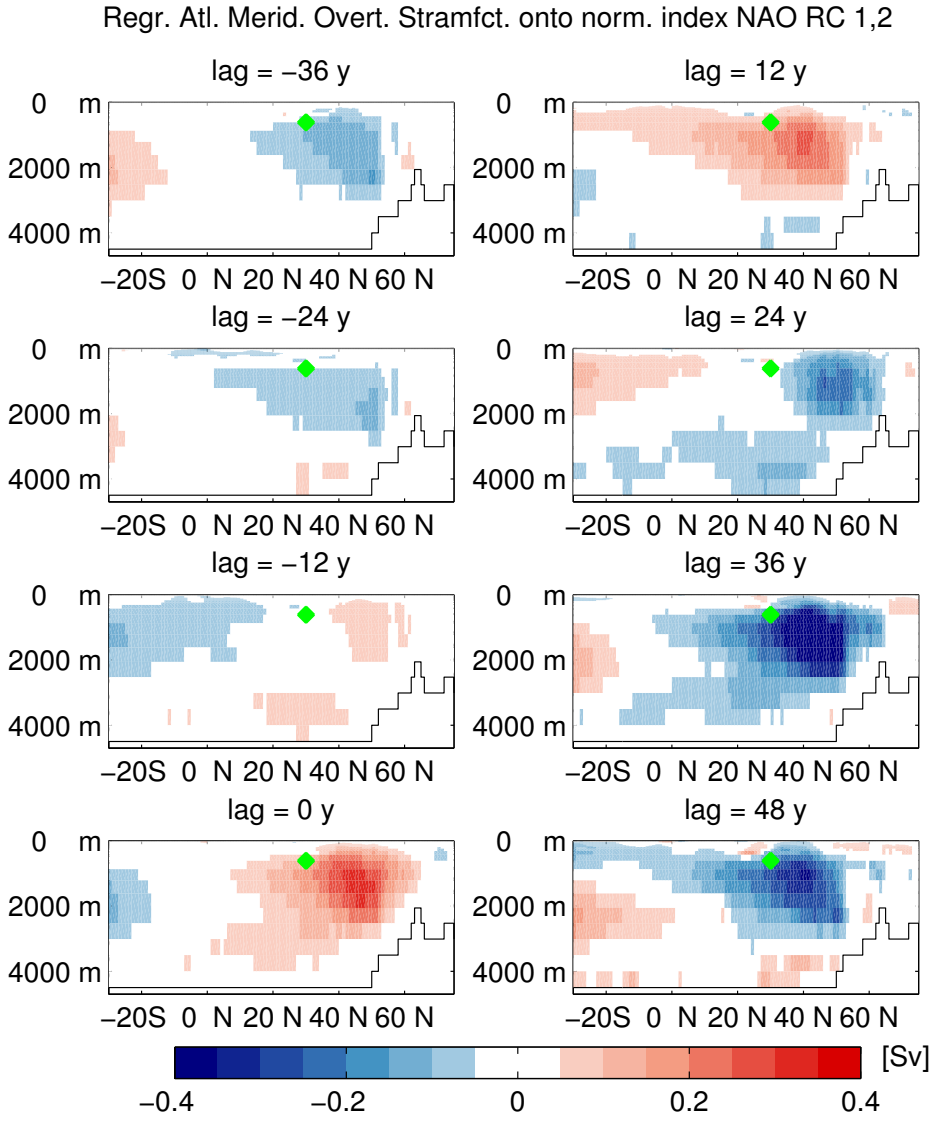

Figure A15: Regression of the Atlantic meridional overturning streamfunction onto the normalized SSA time series reconstructions of the 58 year mode of the NAO index for different lags. Positive lags indicate that the index is leading. The green dot indicates where the AMOC 30°N index is located.

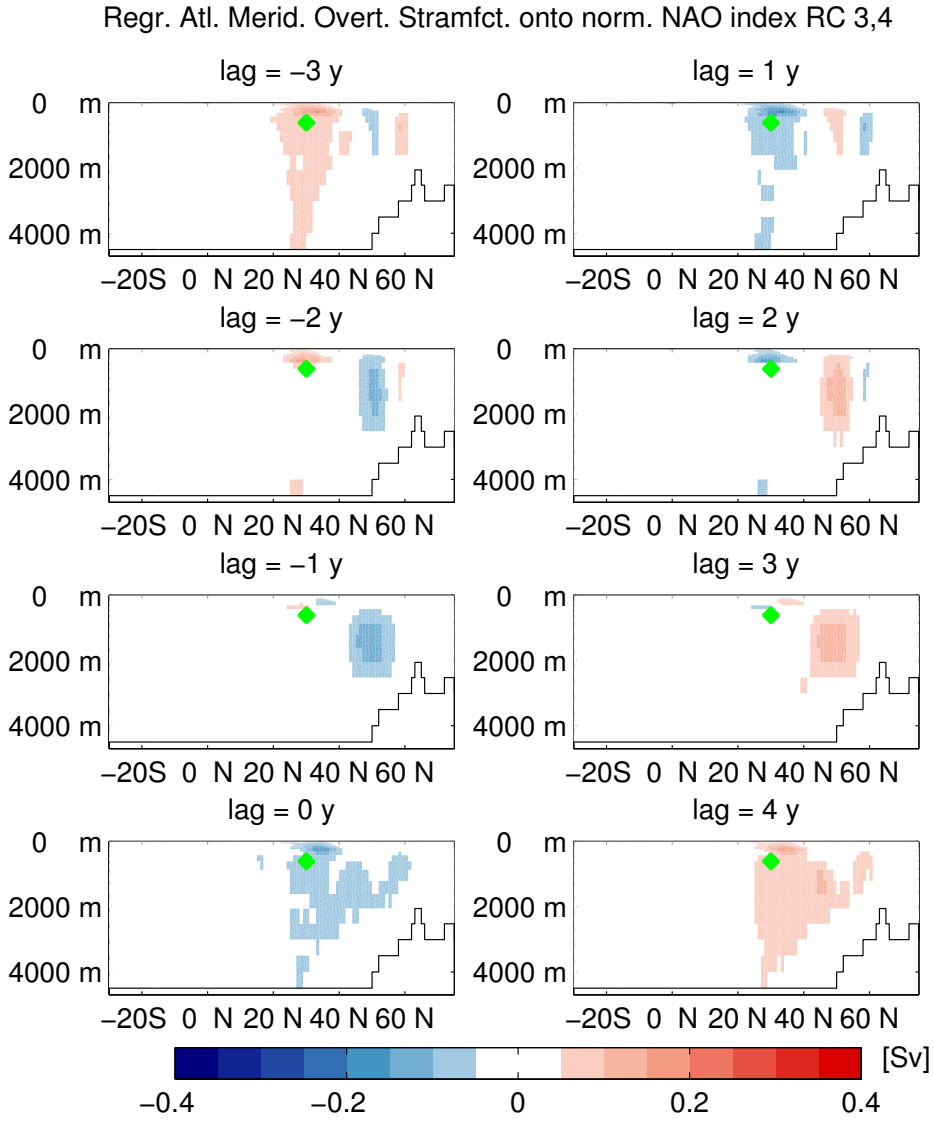

Figure A16: Regression of the Atlantic meridional overturning streamfunction onto the normalized SSA time series reconstructions of the 8 year mode of the NAO index for different lags. Positive lags indicate that the index is leading. The green dot indicates where the AMOC 30°N index is located.

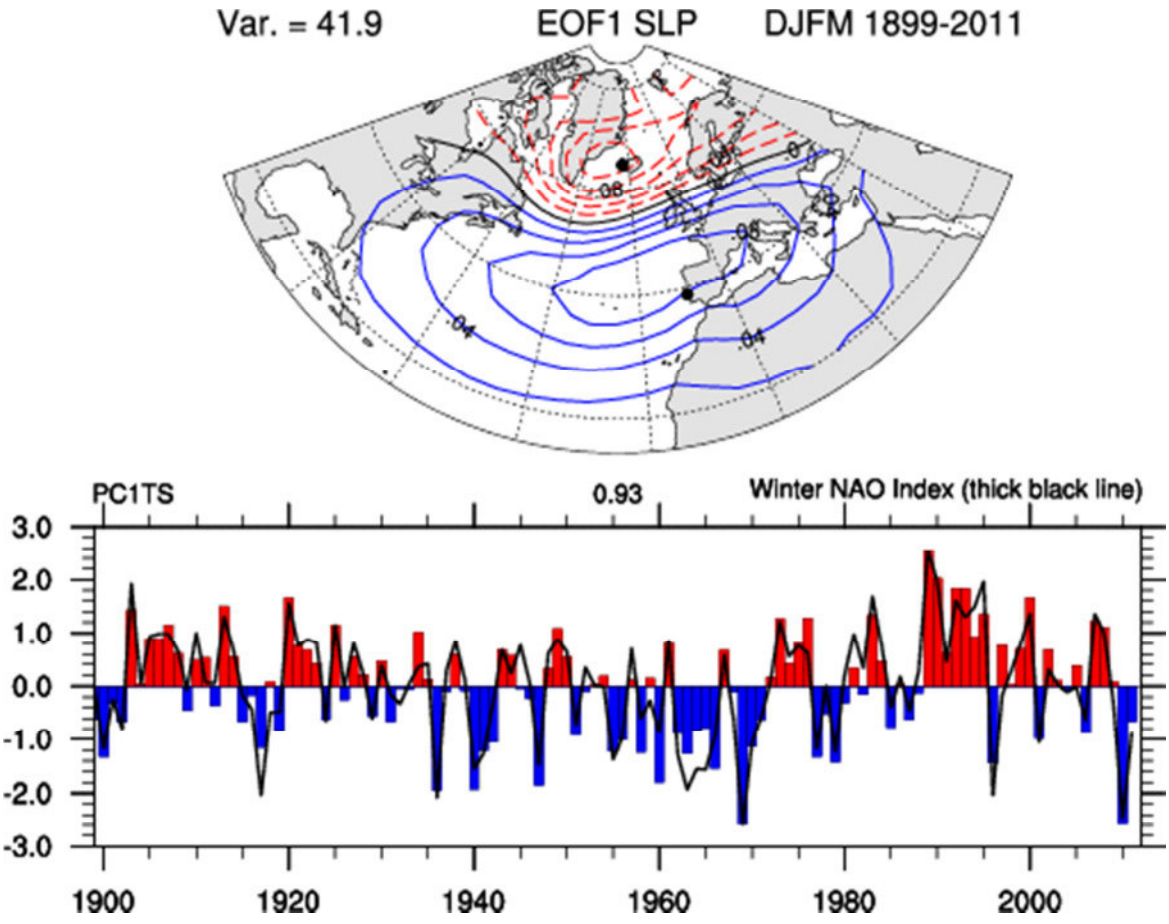

Figure A17: PC-based Hurrell NAO pattern and index time series. From: https://climatedataguide.ucar.edu/climate-data/hurrell-north-atlantic-oscillation-nao-index-pc-based

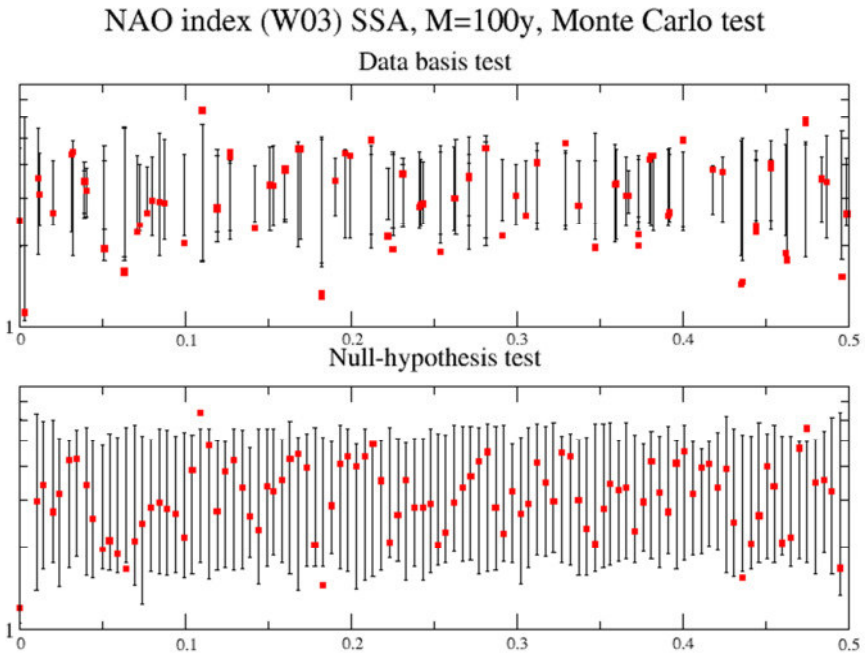

Figure A18: Power of the different SSA frequency modes of the NAO index in the control experiment. The bars indicate the 95%-confidence interval of a red noise process derived from 100 Monte Carlo realizations. In the upper panel a data-adaptive and in the lower panel a null hypothesis-based test was carried out.

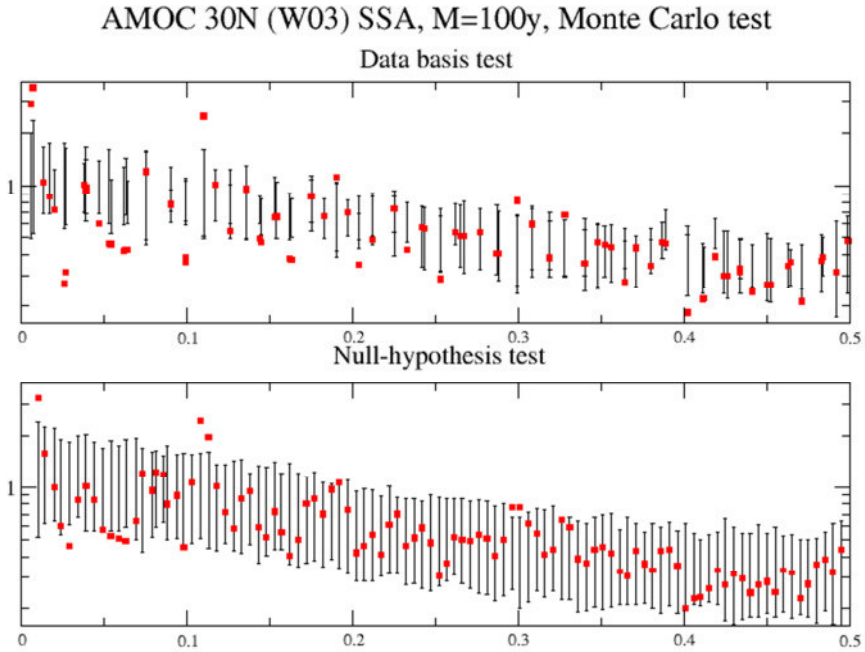

Figure A19: Power of the different SSA frequency modes of the AMOC 30°N index in the control experiment. The bars indicate the 95%-confidence interval of a red noise process derived from 100 Monte Carlo realizations. In the upper panel a data-adaptive and in the lower panel a null hypothesis-based test was carried out.

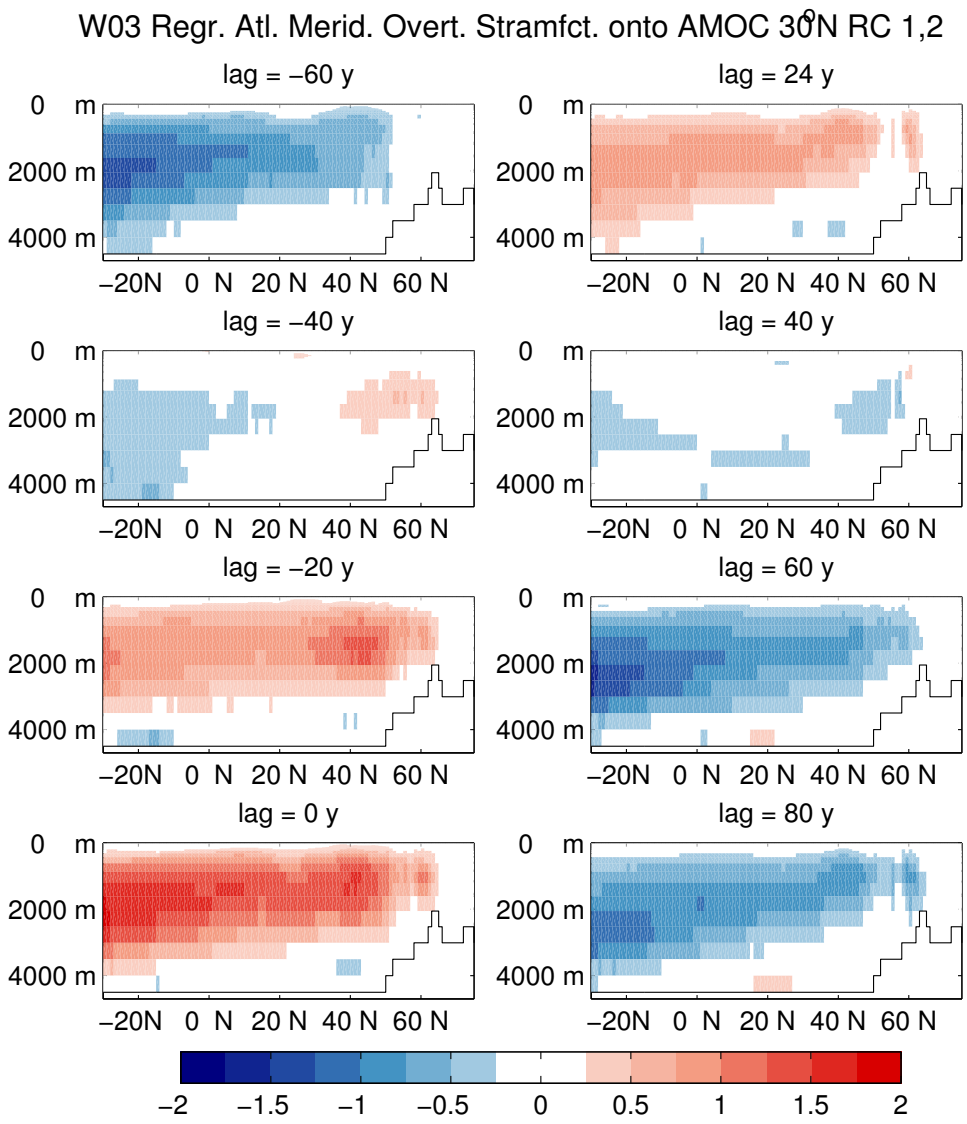

Figure A20: SSA results in the W03 control experiment (years 300 to 999): Regression of the Atlantic meridional overturning streamfunction onto the normalized SSA time series reconstructions of the 150 year mode of the AMOC 30°N index. Different lags are shown. Positive lags indicate that the index is leading.

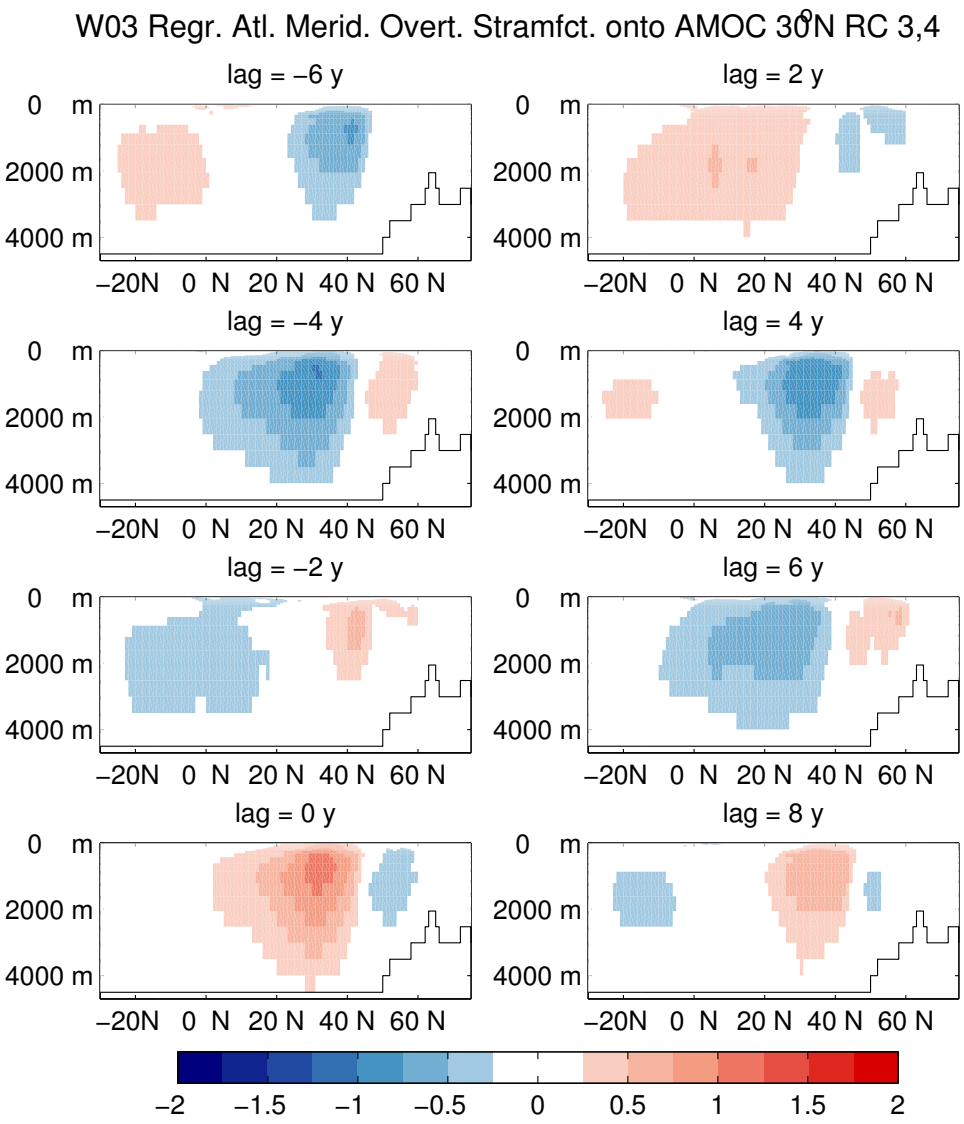

Figure A21: SSA results in the W03 control experiment (years 300 to 999): Regression of the Atlantic meridional overturning streamfunction onto the normalized SSA time series reconstructions of the 9 year mode of the AMOC 30°N index. Different lags are shown. Positive lags indicate that the index is leading.

REFERENCES

Allen, M. R., and A. W. Robertson (1996), Distinguishing modulated oscillations from coloured noise in multivariate datasets, *Clim. Dyn.*, *12*(11), 775–784, doi:10.1007/s003820050142.

Álvarez-García, F., M. Latif, and A. Biastoch (2008), On Multidecadal and Quasi-Decadal North Atlantic Variability, *J. Clim.*, *21*(14), 3433–3452, doi:10.1175/2007JCLI1800.1.

Ba, J., N. S. Keenlyside, W. Park, M. Latif, E. Hawkins, and H. Ding (2013), A mechanism for Atlantic multidecadal variability in the Kiel Climate Model, *Clim. Dyn.*, *41*(7-8), 2133–2144, doi:10.1007/s00382-012-1633-4.

Bacon, S., W. J. Gould, and Y. L. Jia (2003), Open-ocean convection in the Irminger Sea, *Geophys. Res. Lett.*, *30*(5), 1246, doi:10.1029/2002GL016271.

Bjerknes, J. (1964), Atlantic Air-Sea Interaction, *Adv. Geophys.*, *10, 1-82*.

Cunningham, S. A. et al. (2007), Temporal variability of the Atlantic meridional overturning circulation at 26.5 degrees N., *Science*, *317*(5840), 935–938, doi:10.1126/science.1141304.

Czaja, A., A. W. Robertson, and T. Huck (2003), The role of Atlantic ocean-atmosphere coupling in affecting North Atlantic Oscillation variability, *Geophys. Monogr. Ser.*, *134*, 147–172, doi:10.1029/134GM07.

Delworth, T. L., and R. J. Greatbatch (2000), Multidecadal thermohaline circulation variability driven by atmospheric surface flux forcing, *J. Clim.*, 13(9), 1481–1495, doi:10.1175/1520-0442(2000)013<1481:MTCVDB>2.0.CO;2.

Dettinger, M. D., M. Ghil, C. M. Strong, W. Weibel, and P. Yiou (1995), Software Expedites Singular-Spectrum Analysis of Noisy Time Series, *Trans. Am. Geophys. Union*, *76*(2), 12-21, doi:10.1029/EO076i002p00012.

Eden, C., and J. Willebrand (2001), Mechanism of Interannual to Decadal Variability of the North Atlantic Circulation, *J. Clim.*, 14(*10)*, 2266–2280, doi:10.1175/1520-0442(2001)014<2266:MOITDV>2.0.CO;2.

Eden, C., R. J. Greatbatch, and C. W. Böning (2004), Adiabatically Correcting an Eddy-Permitting Model Using Large-Scale Hydrographic Data: Application to the Gulf Stream and the North Atlantic Current, *J. Phys. Oceanogr.*, *34*(4), 701–719, doi:10.1175/1520-0485(2004)034<0701:ACAEMU>2.0.CO;2.

Ganachaud, A., and C. Wunsch (2003), Large-Scale Ocean Heat and Freshwater Transports during the World Ocean Circulation Experiment, *J. Clim.*, *16*(4), 696–705, doi:10.1175/1520-0442(2003)016<0696:LSOHAF>2.0.CO;2.

Ghil, M., and R. Vautard (1991), Interdecadal oscillations and the warming trend in global temperature time series, *Nature*, *350*(6316), 324–327, doi:10.1038/350324a0.

Ghil, M. et al. (2002), Advanced spectral methods for climate time series, *Rev. Geophys.*, *40*(1), 3.1–3.41, doi:10.1029/2001RG000092.

Gillett, N. P., H. F. Graf, and T. J. Osborn (2003), Climate Change and the North Atlantic Oscillation, *Geophys. Monogr. Ser.*, *134*, 193–209, doi:10.1029/134GM09.

Hasselmann, K. (1976), Stochastic climate models Part I. Theory, *Tellus*, *28*(6), 473–485, doi:10.1111/j.2153-3490.1976.tb00696.x.

Hátún, H., A. B. Sandø, H. Drange, B. Hansen, and H. Valdimarsson (2005), Influence of the Atlantic subpolar gyre on the thermohaline circulation., *Science*, *309*(5742), 1841–1844, doi:10.1126/science.1114777.

Hurrell, J. W. (1995), Decadal trends in the north atlantic oscillation: regional temperatures and precipitation., *Science*, *269*(5224), 676–679, doi:10.1126/science.269.5224.676.

Hurrell, J. W., Y. Kushnir, G. Ottersen, and M. Visbeck (2003), An Overview of the North Atlantic Oscillation, *Geophys. Monogr. Ser.*, *134*, 1–35, doi:10.1029/134GM01.

Jolliffe, I. T. (2002), *Principal Component Analysis*, Springer Series in Statistics.

Kalnay, E. et al. (1996), The NCEP/NCAR 40-year reanalysis project, *B. Am. Meteorol. Soc.*, *77*(3), 437–471, doi:10.1175/1520-0477(1996)077<0437:TNYRP>2.0.CO;2.

Kuhlbrodt, T., A. Griesel, M. Montoya, A. Levermann, M. Hofmann, and S. Rahmstorf (2007), On the driving processes of the Atlantic meridional overturning circulation, *Rev. Geophys.*, *45*(2), RG2001, doi:10.1029/2004RG000166.

Kushnir, Y., W. A. Robinson, I. Bladé, N. M. J. Hall, S. Peng, and R. Sutton (2002), Atmospheric GCM Response to Extratropical SST Anomalies: Synthesis and Evaluation, *J. Clim.*, *15*(16), 2233–2256, doi:10.1175/1520-0442(2002)015<2233:AGRTES>2.0.CO;2.

Kwon, Y.-O., and C. Frankignoul (2012), Stochastically-driven multidecadal variability of the Atlantic meridional overturning circulation in CCSM3, *Clim. Dyn.*, *38*(5-6), 859–876, doi:10.1007/s00382-011-1040-2.

Latif, M., and C. W. Böning, J. Willebrand, A. Biastoch, F. Álvarez-García, N. Keenlyside, and H. Pohlmann (2007), Decadal to multidecadal variability of the Atlantic MOC: mechanisms and predictability, *Geophys. Monogr. Ser.*, *173*, 149–166, doi:10.1029/173GM11.

Latif, M., T. Martin, and W. Park (2013), Southern Ocean Sector Centennial Climate Variability and Recent Decadal Trends, *J. Clim.*, *26*(19), 7767–7782, doi:10.1175/JCLI-D-12-00281.1.

Levitus, S., T.P. Boyer, M.E. Conkright, T. O' Brien, J. I. Antonov, C. Stephens, L. Stathoplos, D. Johnson, and R. Gelfeld (1998), NOAA Atlas NESDIS 18, World Ocean Database 1998: VOLUME 1: INTRODUCTION, *U.S. Gov. Print. Off. Wash., D.C.*

Madec, G., P. Delecluse, M. Imbard, and C. Lévy (1998), OPA 8.1 Ocean General Circulation Model reference manual, *Note du Pole modélisation 11. Inst. Pierre-Simon Laplace*, 91 pp.

Marshall, J., and F. Schott (1999), Open-ocean convection: Observations, theory, and models, *Rev. Geophys.*, 37(1), 1–64, doi:10.1029/98RG02739.

Martin, T., W. Park, and M. Latif (2012), Multi-centennial variability controlled by Southern Ocean convection in the Kiel Climate Model, *Clim. Dyn.*, *40*(7-8), 2005–2022, doi:10.1007/s00382-012-1586-7.

Osborn, T. J. (2011), *Variability and changes in the North Atlantic Oscillation index. In Hydrological, socioeconomic and ecological impacts of the North Atlantic Oscillation in the Mediterranean region* (eds. Vicente-Serrano S. M. and R. M. Trigo), Springer, doi:10.1007/978-94-007-1372-7.

Park, W., and M. Latif (2008), Multidecadal and multicentennial variability of the meridional overturning circulation, *Geophys. Res. Lett.*, *35*(22), L22703, doi:10.1029/2008GL035779.

Park, W., and M. Latif (2010), Pacific and Atlantic multidecadal variability in the Kiel Climate Model, *Geophys. Res. Lett.*, *37*(24), L24702, doi:10.1029/2010GL045560.

Park, W., and M. Latif (2012), Atlantic Meridional Overturning Circulation response to idealized external forcing, *Clim. Dyn.*, *39*(7-8), 1709–1726, doi:10.1007/s00382-011-1212-0.

Park, W., N. Keenlyside, M. Latif, A. Ströh, R. Redler, E. Roeckner, and G. Madec (2009), Tropical Pacific Climate and Its Response to Global Warming in the Kiel Climate Model, *J. Clim.*, *22*(1), 71–92, doi:10.1175/2008JCLI2261.1.

Pickart, R. S., and M. A. Spall (2007), Impact of Labrador Sea Convection on the North Atlantic Meridional Overturning Circulation, *J. Phys. Oceanogr.*, *37*(9), 2207–2227, doi:10.1175/JPO3178.1.

Pickart, R. S., D. J. Torres, and R. A. Clarke (2002), Hydrography of the Labrador Sea during active convection, *J. Phys. Oceanogr., 32(2),* 428–457, doi:10.1175/1520-0485(2002)032<0428:HOTLSD>2.0.CO;2.

Roberts, C. D., F. K. Garry, and L. C. Jackson (2013), A Multimodel Study of Sea Surface Temperature and Subsurface Density Fingerprints of the Atlantic Meridional Overturning Circulation, *J. Clim.*, *26*(22), 9155–9174, doi:10.1175/JCLI-D-12-00762.1.

Roeckner, E. et al. (2003), The atmospheric general circulation model ECHAM5. Part I: Model description, *Max Planck Inst. Meteorol. Rep. 349.*

Schmittner, A., M. Latif, and B. Schneider (2005), Model projections of the North Atlantic thermohaline circulation for the 21st century assessed by observations, *Geophys. Res. Lett.*, *32*, L23710, doi:10.1029/2005GL024368.

Smith, R. D., M. E. Maltrud, F. O. Bryan, and M. W. Hecht (2000), Numerical simulation of the North Atlantic Ocean at 1/10°, *J. Phys. Oceanogr.*, *30(7)*, 1532–1561, doi:10.1175/1520-0485(2000)030<1532:NSOTNA>2.0.CO;2.

Uppala, S. M. et al. (2005), The ERA-40 re-analysis, *Q. J. R. Meteorol. Soc.*, *131*(612), 2961–3012, doi:10.1256/qj.04.176.

Valcke, S. (2006), OASIS3 user guide, *Prism Tech. Rep. 3*.

Vautard, R., and M. Ghil (1989), Singula spectrum analysis in nonlinear dynamics, with applications to paleo-climatic time series, *Physica D*, *35*, 395–424, doi::10.1016/0167-2789(89)90077-8.

Vautard, R., M. Ghil, and P. Yiou (1992), Singular-spectrum analysis: A toolkit for short, noisy chaotic signals, *Physica D*, *58*(1-4), 95–126, doi:10.1016/0167-2789(92)90103-T.

Visbeck, M., E. P. Chassignet, R. G. Curry, T. L. Delworth, R. R. Dickson, and G. Krahmann (2003), The ocean's response to North Atlantic Oscillation variability, *Geophys. Monogr. Ser.*, *134*, 113–145, doi:10.1029/134GM06.

Walker, G. T. (1924), Correlation in seasonal variations of weather, IX. A further study of world weather, *Mem. India Meteorol. Dep.*, *24*(9), 275–333.

Zhu, X., and J. Jungclaus (2008), Interdecadal variability of the meridional overturning circulation as an ocean internal mode, *Clim. Dyn.*, *31*(6), 731–741, doi:10.1007/s00382-008-0383-9.

THESIS STATEMENT

I hereby confirm that I have independently written this master thesis and that no other than the indicated aids and sources have been used. I also confirm that the printed version is the same as the version provided on the CD-ROM.